Structural and Functional Characterization of a Fish Type I Subgroup d IFN Reveals Its Binding to Receptors

Yanyun Guan,*,[1] Jingjie Chen,*,[1] Hongxin Guan,[†] Tao-Tao Chen,[†] Yan Teng,* Zuyun Wei,* Zekai Li,[†] Songying Ouyang,[†] and Xinhua Chen*,[‡]

Teleost fish type I IFNs and the associated receptors from the cytokine receptor family B (CRFB) are characterized by remarkable diversity and complexity. How the fish type I IFNs bind to their receptors is still not fully understood. In this study, we demonstrate that CRFB1 and CRFB5 constitute the receptor pair through which type I subgroup d IFN (IFNd) from large yellow croaker, *Larimichthys crocea*, activates the conserved JAK-STAT signaling pathway as a part of the antiviral response. Our data suggest that *L. crocea* IFNd (*Lc*IFNd) has a higher binding affinity with *L. crocea* CRFB5 (*Lc*CRFB5) than with *Lc*CRFB1. Furthermore, we report the crystal structure of *Lc*IFNd at a 1.49-Å resolution and construct structural models of *Lc*IFNd in binary complexes with predicted structures of extracellular regions of *Lc*CRFB1 and *Lc*CRFB5, respectively. Despite striking similarities in overall architectures of *Lc*IFNd and its ortholog human IFN-ω, the receptor binding patterns between *Lc*IFNd and its receptors show that teleost and mammalian type I IFNs may have differentially selected helices that bind to their homologous receptors. Correspondingly, key residues mediating binding of *Lc*IFNd to *Lc*CRFB1 and *Lc*CRFB5 are largely distinct from the receptor-interacting residues in other fish and mammalian type I IFNs. Our findings reveal a ligand/receptor complex binding mechanism of IFNd in teleost fish, thus providing new insights into the function and evolution of type I IFNs. ***The Journal of Immunology*****, 2024, 212: 1207–1220.**

Type I IFNs are a family of cytokines specialized in coordinating immune responses against viruses and other intracellular pathogens (1–4). In mammals, all type I IFNs bind to the cell surface receptor formed by IFN-α/β receptor (IFNAR) subunits 1 and 2 (IFNAR1 and IFNAR2) (5–7), which activates the JAK-STAT signaling pathway, resulting in the transcription of various IFN-stimulated genes (ISGs) (8, 9). The type I IFN receptor subunits IFNAR1 and IFNAR2 are both single-transmembrane receptors in which the fibronectin III subdomains are essential for the interaction with IFNs. IFNAR1 has an extracellular region composed of four fibronectin III subdomains (SD1–SD4), whereas IFNAR2 has two fibronectin III subdomains (SD1 and SD2). The crystal structures of the IFN-α/ and IFN-ω/IFNAR1/IFNAR2 ternary complexes have provided a comprehensive understanding of the binding and complex assembly mechanisms between mammalian type I IFNs and their receptors (10–14).

Teleost fish possess a complex, evolutionary divergent type I IFN system that mediates defense against viral infection through the conserved JAK-STAT signaling pathway (15–17). Teleost type I IFNs are divided into two groups based on the number of cysteine residues forming disulfide bonds: group I IFNs (subgroups a, d, e, and h) contain two cysteine residues, whereas group II IFNs (subgroups b, c, f, and i) contain four cysteine residues (18). Fish type I IFN receptors belong to the cytokine receptor family B (CRFB) with 17 known orthologs of mammalian IFNARs (19). From an evolutionary perspective, fish CRFB1/CRFB2 and CRFB5 are equivalent to the mammalian IFNAR2 and IFNAR1, respectively. However, unlike mammalian IFNAR1, the extracellular regions of CRFB5 and other known CRFBs possess only two fibronectin III subdomains, implying differences in the receptor binding mechanism. Previous studies have suggested that teleost group I and group II type I IFNs signal through the CRFB1–CRFB5 and CRFB2–CRFB5 receptor complexes, respectively (20–22). Interestingly, a recent study has shown that grass carp (*Ctenopharyngodon idella*) type I subgroup a IFN (*Ci*IFNa) binds not only to CRFB1 and CRFB5, but also to CRFB2, and that CRFB1 may also form a heterodimeric receptor complex with CRFB2 (23). These findings imply that interactions between

*State Key Laboratory of Mariculture Breeding, Key Laboratory of Marine Biotechnology of Fujian Province, College of Marine Sciences, Fujian Agriculture and Forestry University, Fuzhou, China; [†]Key Laboratory of Microbial Pathogenesis and Interventions–Fujian Province University, The Key Laboratory of Innate Immune Biology of Fujian Province, Biomedical Research Center of South China, Key Laboratory of OptoElectronic Science and Technology for Medicine of the Ministry of Education, College of Life Sciences, Fujian Normal University, Fuzhou, China; and [‡]Southern Marine Science and Engineering Guangdong Laboratory (Zhuhai), Zhuhai, China

[1]Y.G. and J.C. contributed equally to this work.

ORCIDs: 0000-0002-0660-2841 (T.-T.C.); 0009-0009-4736-1456 (Y.T.); 0000-0002-1120-1524 (S.O.); 0000-0003-2379-7596 (X.C.).

Received for publication October 2, 2023. Accepted for publication January 16, 2024.

This work was supported by National Key Research and Development Program of China Grants 2022YFD2401001 and 2021YFC2301403, National Natural Science Foundation of China Grants U1905204, 82225028 and 82172287, China Agriculture Research System of MOF and MARA Grant CARS-47, Institute of Oceanology of Fuzhou (2021F02), Fujian Ocean Synergy Alliance (FOCAL2023-0105).

The crystal structure presented in this article has been submitted to Protein Data Bank under accession number 8IRQ.

Y.G. and J.C. designed and performed most of the experiments with the help of H.G., T.-T.C., Y.T., Z.W., and Z.L.; and J.C. wrote the manuscript with the help of X.C. and S.O., and the other authors made comments and suggestions on the manuscript.

Address correspondence and reprint requests to Prof. Xinhua Chen or Prof. Songying Ouyang, Fujian Agriculture and Forestry University, No. 15 Shangxiadian Road, Fuzhou 350002, China (X.C.) or Fujian Normal University, Fuzhou 350117, China (S.O.). E-mail addresses: chenxinhua@tio.org.cn (X.C.) or ouyangsy@fjnu.edu.cn (S.O.)

The online version of this article contains supplemental material.

Abbreviations used in this article: *Ci*IFNa, Ctenopharyngodon idella IFNa; CPE, cytopathic effect; CRFB, cytokine receptor family B; EPC, epithelioma papulosum cyprinid; Ex, extracellular region; GS, grouper spleen; hIFN, human IFN; HSQC, heteronuclear single quantum coherence; IFNAR, IFN-α/β receptor; IFNa, type I subgroup a IFN; IFNd, type I subgroup d IFN; IFNi, type I subgroup i IFN; ISG, IFN-stimulated gene; ITC, isothermal titration calorimetry; *Lc*CRFB, Larimichthys crocea CRFB; LcIFNd, Larimichthys crocea IFNd; *Lc*IFNi, Larimichthys crocea IFNi; MαC-D, multiple-residue mutations of the helices C and D; MαE, multiple-residue mutations of helix E; mIFN-β, mouse IFN-β; nanoDSF, nano differential scanning fluorimetry; NCR, negatively charged region; NMR, nuclear magnetic resonance; pAb, polyclonal Ab; PCR, positively charged region; PKL, primary head kidney leukocyte; SGIV, Singapore grouper iridovirus; zIFN, zebrafish IFN.

https://doi.org/10.4049/jimmunol.2300651

teleost type I IFNs and their receptors might be more complex than expected. Nevertheless, to which receptors fish type I IFNs bind and how remain poorly studied.

To date, three-dimensional structures of several fish type I IFNs have been reported, including zebrafish IFN (zIFN)-φ1, zIFN-φ2 (24), large yellow croaker (*Larimichthys crocea*) type I subgroup i IFN (IFNi) (*Lc*IFNi) (18), and *Ci*IFNa (23), all of which share a similar structure consisting of six α helices (A–F) and a straight helix F. The ternary complex model of *Lc*IFNi and its receptors CRFB2–CRFB5 based on the homologous ternary complex structure has been constructed, shedding light on the mechanisms by which a fish group II type I IFN binds to their receptors (18). Additionally, structural analysis of *Ci*IFNa has identified the key residues involved in its interaction with receptors (23). Structural data are therefore highly desirable, as they can provide detailed information on molecular mechanisms through which fish type I IFN bind to their receptors.

Our previous study identified type I subgroup d IFN (IFNd) from *L. crocea* (*Lc*IFNd) that showed antiviral activity and regulated the IFN response (25). In this study, we demonstrate that *Lc*IFNd interacts with the receptors *Lc*CRFB1 and *Lc*CRFB5, binding to *Lc*CRFB5 with a higher affinity than binding to *Lc*CRFB1. We also report the crystal structure of *Lc*IFNd, which displays characteristic fish type I group I IFN architecture. Using nuclear magnetic resonance (NMR) titration, homology modeling, and mutational analysis coupled with pull-down assays, we identify key regions and residues of *Lc*IFNd involved in interaction with *Lc*CRFB1 and *Lc*CRFB5. Moreover, using receptor-blocking experiments, we show that *Lc*IFNd triggers the antiviral function through the conserved JAK-STAT signaling pathway by binding to *Lc*CRFB1 and *Lc*CRFB5, and we confirm that the amino acids L18, F43, K113, H128, H135, and M152 of *Lc*IFNd are indispensable for the *Lc*IFNd-mediated JAK-STAT signaling pathway.

Materials and Methods

Primary cells and cell lines

The primary head kidney leukocytes (PKLs) of *L. crocea* were prepared as described previously (26, 27). The continuous epithelioma papulosum cyprini (EPC) cell line was preserved in our laboratory and cultured at 25°C in L-15 medium supplemented with 10% FBS. Grouper spleen (GS) cells were derived from the spleen of orange-spotted grouper (*Epinephelus coioides*) and maintained in L-15 medium supplemented with 10% FBS at 25°C. Singapore grouper iridovirus (SGIV) was propagated in GS cells as previous described (28), and the virus stock was stored at −80°C until use. GS cells and SGIV were gifts from Prof. Qiwei Qin in South China Agricultural University. Human embryonic kidney 293T cells were grown in DMEM (Life Technologies) containing 10% FBS, 100 U/ml penicillin, and 100 μg/ml streptomycin (Life Technologies) at 37°C in a 5% CO_2 atmosphere.

Plasmid construction, expression, and purification of Lc*IFNd*

The *Lc*IFNd gene fragment encoding the mature peptide sequence (residues 21–185; API68651) was amplified with primer set (Supplemental Table I) from the *L. crocea* spleen cDNA using RT-PCR. The *Lc*IFNd gene fragment was cloned into the expression vector pET28a with N-terminal 6× His and Sumo-tag, and the recombinant vector was transformed into BL21(DE3) pLysS-competent cells (EC1002M, WEIDI). Protein expression was induced with 300 mM isopropyl β-D-thiogalactoside at 18°C and 220 rpm for 16 h. Afterward, the cells were collected and lysed in lysis buffer (25 mM Tris-HCl [pH 7.5], 150 mM NaCl, 2 mM β-ME). r*Lc*IFNd was purified using Ni-NTA affinity chromatography, followed by gel-filtration chromatography using a Superdex 75 Increase column (Cytiva) (Supplemental Fig. 1A).

Crystallization

Purified *Lc*IFNd was concentrated to 10 mg/ml in a buffer containing 20 mM HEPES (pH 7.5) and 150 mM NaCl. Crystals were grown at 16°C using the sitting drop vapor diffusion method with 0.8 μl of recombinant protein and 0.8 μl of reservoir solution (0.1 M Tris-HCl [pH 7.0] and 20% polyethylene glycol 2000). The crystals were harvested in the reservoir solution supplemented with 15–20% glycerol and flash-frozen in liquid nitrogen.

X-ray diffraction data collection and structure determination

Crystal diffraction data for *Lc*IFNd were collected at the Shanghai Synchrotron Radiation Facility (SSRF) BL-02U1 using the single-wavelength anomalous diffraction method. Datasets were processed on-site with the HKL-2000 package. The AutoSol program of the Phenix package was used for single-wavelength anomalous diffraction phasing, followed by iterative manual building using Coot and refinement in Phenix (29, 30). The crystals belong to space group P 1 21 1 with unit-cell dimensions of $a = 40.378$ Å, $b = 38.813$ Å, and $c = 51.091$ Å. The final structure was refined to 1.49-Å resolution (Table I). Structure quality was analyzed during refinement in Phenix and later validated in the PDB validation server. Structural figures were generated using PyMOL (Schrödinger, LLC). The crystal structure has been deposited in the PDB (https://www.rcsb.org/structure/unreleased/8IRQ) under accession number 8IRQ. In the crystal structure of the *Lc*IFNd, 11 residues (aa 29–39) were not observed in the electron density. However, given that structure of *Lc*IFNd predicted by AlphaFold v2.0 is almost entirely consistent with the crystal structure of *Lc*IFNd (root-mean-square deviation of 0.377) (Supplemental Fig. 1B), the missing segment can be surmised to be a flexible loop between structural elements A and B with a high confidence. For the convenience of research, the predicted *Lc*IFNd structure model was used as a research model in this study (Supplemental Fig. 1B, left panel).

Nano differential scanning fluorimetry

The thermostability of *Lc*IFNd with a cysteine mutation was determined using the nano differential scanning fluorimetry (nanoDSF) method based on intrinsic tryptophan and tyrosine fluorescence. All nanoDSF assays were performed using the Prometheus NT.48 instrument (NanoTemper Technologies). Samples (~10 μl at 0.5–1 mg/ml) were loaded into standard-grade nanoDSF capillaries, placed on the Prometheus capillary holder, and subjected to a temperature ramping of 1°C/min from 20 to 94.8°C. For a more detailed description of the principle of the nano-DSF assay, please refer to Chen et al. (18).

Luciferase reporter assay

The promoter region (located at 29555747–29557148 bp of the *L. crocea* genome; GenBank accession no. LT972194.1) (31) of the *L. crocea* MxA gene was inserted into the Dual-Luciferase reporter plasmid pGL3-basic for the luciferase reporter assay. Sequences encoding CRFB1 (OM864520), CRFB2 (OM864521), CRFB3 (OM864522), CRFB4 (OM864523), and CRFB5 (OM864524) were cloned separately into the pcDNA3.1 vector. EPC cells were seeded at 2×10^4 cells per well into 96-well culture plates and grown to 80% confluence overnight at 28°C in Opti-MEM supplemented with 10% FBS, 100 μg/ml streptomycin, and 200 U/ml penicillin G. The prepared cells were transfected with 100 μl of medium containing 50 ng of pGL3-MxA, 50 ng of one of the pcDNA3.1-CRFB vectors or empty pcDNA3.1 plasmid, and 1 ng of pRL-TK using the FuGENE HD transfection reagent (Promega) according to the manufacturer's protocol. The cells were stimulated with 250 ng/ml r*Lc*IFNd or control protein (Nus-tag) 48 h after transfection. Luciferase activity was measured 24 h poststimulation using the Dual-Luciferase reporter assay system (Promega). The relative luciferase activity of the MxA promoter was calculated by comparing the normalized luciferase activity in *Lc*IFNd-treated cells with that in control protein–treated cells. All data were obtained from three independent experiments. Values significantly different from all controls are shown as $*p < 0.05$ and $**p < 0.01$.

Pull-down assays

Pull-down experiments were used to determine the interaction of *Lc*IFNd with *Lc*CRFB1 and *Lc*CRFB5, respectively, and performed as previously described (18). The GST-tagged *Lc*IFNd was expressed in *Escherichia coli*. Gene fragments encoding an extracellular region (Ex) of the receptor subunits *Lc*CRFB1 (residues 20–220) and *Lc*CRFB5 (residues 17–234) were subcloned into pFastbac1 vectors containing the hemotin signal peptide. Recombinant *Lc*CRFB1-Ex (C-terminal His-tag) and *Lc*CRFB5-Ex (N-terminal Flag-tag and C-terminal His-tag) were expressed in the insect cell/baculovirus system and purified from the Hi5 cell supernatant with a Ni-NTA affinity chromatography column (Cytiva). The pull-down assays were performed using glutathione Sepharose beads (P2253, Beyotime) by incubating purified GST-tagged *Lc*IFNd protein with His-tagged *Lc*CRFB1-Ex or Flag-tagged *Lc*CRFB5-Ex, respectively. The beads were washed with wash buffer (25 mM HEPES [pH 7.5], 100 mM NaCl, 3 mM β-ME, 0.2% Triton X-100), followed by elution with buffer (20 mM reduced glutathione, 25 mM HEPES [pH 7.5], 100 mM NaCl, 3 mM β-ME, 0.2% Triton X-100). Eluted fractions were used for Western blot analysis. Western blot was performed using GST-tag mouse mAb (T0007, Affinity Biosciences), His-tag mouse mAb (T0009,

Affinity Biosciences), or Flag-tag mouse mAb (T0003, Affinity Biosciences) as the primary Abs, and goat anti-mouse IgG (H+L) HRP (S0002, Affinity Biosciences) as the secondary Ab.

Isothermal titration calorimetry

The affinity experiments were performed in low-volume Nano isothermal titration calorimetry (ITC) (TA Instruments). *Lc*IFNd, *Lc*CRFB1-Ex, and *Lc*CRFB5-Ex samples were prepared as described above. All samples for the assays were prepared in a buffer containing 20 mM HEPES (pH 7.5) and 150 mM NaCl. To measure the affinity between *Lc*IFNd and *Lc*CRFB1-Ex, 100 μM *Lc*IFNd in the syringe was titrated into a sample cell containing 30 μM *Lc*CRFB1-Ex. To determine the affinity between *Lc*IFNd and *Lc*CRFB5-Ex, 60 μM *Lc*IFNd in a syringe was titrated into a sample cell containing 50 μM *Lc*CRFB5-Ex. In addition, the affinity between *Lc*CRFB1-Ex and *Lc*CRFB5-Ex was also determined. All experiments were carried out at 25°C. Data correction and analysis were performed using NanoAnalyze software (TA Instruments).

NMR analysis

*Lc*IFNd (residues 21–185) was cloned into the pET-28a vector with a 6× His tag. The r*Lc*IFNd protein was then expressed overnight at 18°C in BL21(DE3) cells in M9 minimal media (32) with 1 g/l ^{15}N-NH_4Cl and 4 g/l ^{13}C-glucose as the nitrogen and carbon sources, respectively. The expressed 6× His-tagged protein was purified as described above, buffer exchanged into 20 mM HEPES (pH 7.0), 100 mM NaCl, and 1 mM DTT, and concentrated to 250 μM. Protein backbone resonances were assigned after analysis of HNCA, HNCOCA, HNCACB, HNCO, and ^{15}N-edited NOESY (nuclear Overhauser effect spectroscopy)–heteronuclear single quantum coherence (HSQC) spectra according to standard protocols (33). To estimate the interaction of the *Lc*IFNd with *Lc*CRFB1-Ex and *Lc*CRFB5-Ex, respectively, *Lc*IFNd samples (250 μM) were titrated into the deuterated *Lc*CRFB1-Ex (250 μM) and *Lc*CRFB5-Ex (250 μM), respectively. *Lc*IFNd+*Lc*CRFB1-Ex and *Lc*IFNd+*Lc*CRFB5-Ex ^{1}H-^{15}N HSQC spectra were assigned via the same experiments, respectively. All NMR spectra were recorded at 298 K on a Bruker Avance III 850-MHz spectrometer, acquired using Bruker TopSpin 3.6.2 software, processed using NMRPipe software (34), and analyzed using Sparky software (35).

Construction of the structural model

The structures of *Lc*CRFB1-Ex and *Lc*CRFB5-Ex were predicted in AlphaFold v2.0 (https://www.alphafold.ebi.ac.uk/). The *Lc*IFNd–*Lc*CRFB1-Ex binary complex structure model was spatially docked in PyMOL. The structures of *Lc*IFNd and *Lc*CRFB5-Ex were aligned with those of IFN-ω and IFNAR2, respectively, to construct the model of the *Lc*IFNd–*Lc*CRFB5-Ex binary complex structure. All structural models were energy minimized using Molecular Operating Environment (MOE) software (36).

Mutant protein–protein interaction assays

The following *Lc*IFNd mutants were used for *Lc*IFNd–*Lc*CRFB1-Ex interaction assays: 1) single-residue mutations: K113A, K114A, H119A, K123A, R124A, H128A, K131A, K132A, and H135A; 2) multiple-residue mutations of helix E (MαE): K113/K114/H119/K123/R124/H128/K131/K132/H135A; and 3) multiple-residue mutations of the helices C and D (MαC-D): E67/E68/E74/E75/D76/E85/E89A. For *Lc*IFNd–*Lc*CRFB5-Ex interaction assays, the following single-residue mutations of *Lc*IFNd were used: R11A, E15A, L18A, D19A, E33A, D34A, D39A, F43A, R144A, K145A, R148A, M152A, D155A, and R162A. All mutations were introduced into GST-tagged *Lc*IFNd using the expression vector pGEX-6P-1. The mutant variants of the GST-tagged *Lc*IFNd were expressed in *Escherichia coli* following the protocol for wild-type *Lc*IFNd described above. His-tagged *Lc*CRFB1-Ex and Flag-tagged *Lc*CRFB5-Ex were expressed in Hi5 cells. Protein interaction was detected by a pull-down assay as described previously (37). Briefly, purified GST-tagged *Lc*IFNd mutants were incubated with His-tagged *Lc*CRFB1-Ex and Flag-tagged *Lc*CRFB5-Ex using His and Flag Sepharose beads (M20008M, Abmart), respectively. The beads were washed with 6 column volumes of wash buffer (25 mM HEPES [pH 7.5], 150 mM NaCl, 3 mM β-ME, 0.2% Triton X-100), after which elution was carried out using elution buffer (as described in *Pull-down assays*). The eluted fractions were used for Western blot analysis. Western blot was performed by using GST-tag mouse mAb (T0007, Affinity Biosciences), His-tag mouse mAb (T0009, Affinity Biosciences), and Flag-tag mouse mAb (T0003, Affinity Biosciences) as the primary Abs, and goat anti-mouse IgG (H+L) HRP (S0002, Affinity Biosciences) as the secondary Ab.

Preparation of polyclonal Abs

Recombinant *Lc*CRFB1-Ex and *Lc*CRFB5-Ex were expressed in the insect cell/baculovirus system and purified from the Hi5 cell supernatant using Ni-NTA affinity chromatography (Cytiva). Purified *Lc*CRFB1-Ex and *Lc*CRFB5-Ex proteins were used for the preparation of polyclonal Abs (pAbs). To prepare the pAbs, 6-wk-old male New Zealand White rabbits were immunized with 250 mg of purified *Lc*CRFB1-Ex and *Lc*CRFB5-Ex, respectively, in CFA (Sigma-Aldrich, F5881). Rabbits were immunized four times at biweekly intervals. The ELISA validation of pAb titers and further purification steps were described in a previous study (18). Nonspecific rabbit Abs were purified from the sera of unimmunized rabbits and used as controls. The obtained pAbs were stored at −80°C until further use.

Verification of pAb specificity

The specificity of anti–*Lc*CRFB5-Ex pAbs has been verified in our previous studies (18). The specificities of anti–*Lc*CRFB1-Ex pAbs were tested by Western blot against r*Lc*CRFB1-Ex and spleen and head kidney tissues obtained from a fresh *L. crocea* specimen. To further confirm the specificity of anti–*Lc*CRFB1-Ex pAbs, immunofluorescence labeling of PKLs and HEK-293T cells was performed with pAbs. The pCMV-HA plasmids were overexpressed in HEK-293T cells as control, and pCMV-HA-*Lc*CRFB1 groups containing full-length *Lc*CRFB1 cDNAs were overexpressed in HEK-293T cells as experimental groups. An indirect immunofluorescence assay was performed as previously described (38). Briefly, the isolated PKLs and pCMV-HA– and pCMV-HA-*Lc*CRFB1–transfected HEK-293T cells were incubated with anti–*Lc*CRFB1-Ex pAbs (1:100) for 50 min. After removing the pAbs, cells were incubated with the Alexa Fluor 488–conjugated goat anti-rabbit IgG (1:200, Invitrogen) as the secondary Ab for 50 min. Finally, PKLs and HEK-293T cells were stained with DAPI (1:100, Invitrogen) fluorescent dyes (10 mg/ml) for 5 min in the dark. The stained PKLs and HEK-293T cells were observed under a laser-scanning confocal microscope (Leica Microsystems, Wetzlar, Germany).

Antiviral activity assays in GS cells

The GS cells were seeded onto six-well plates for 12 h. The cells were pretreated with r*Lc*IFNd at a final concentration of 50 ng/ml or PBS (as a control) for 2 h, after which the cells were infected with SGIV at a multiplicity of infection of 2. At 24 h postinfection, the cells were observed microscopically for a cytopathic effect (CPE) (Leica Microsystems, Wetzlar, Germany). Infected cells were then harvested at 12 and 24 h postinfection for the analysis of viral gene expression by real-time quantitative PCR.

Gene expression analysis by real-time quantitative PCR

To study the effects of *Lc*IFNd on the JAK-STAT signaling pathway in vitro, 5×10^6 PKLs were stimulated with r*Lc*IFNd (250 ng/ml) or BSA (as control; 250 ng/ml) for 6 or 12 h at 28°C. The cultured cells were then sampled for total RNA extraction using the Eastep super total RNA extraction kit (Promega). The cDNA was synthesized using GoScript reverse transcription mix (Promega) with oligo(dT) primers (Supplemental Table I). Then, cDNA samples were diluted to a suitable concentration in nuclease-free water for real-time PCR. The two virus SGIV genes (MCP and VP19) and JAK1, IRF9, STAT1, STAT2, MxA, PKR, and viperin from *L. crocea* were obtained from the National Center for Biotechnology Information GenBank (https://www.ncbi.nlm.nih.gov/genbank/). Real-time PCR was analyzed using TB Green mix (Takara) and specific primers in a QuantStudio 5 real-time PCR system (Thermo Fisher Scientific). All reactions were performed in triplicate on 96-well plates. Gene expression levels were normalized against the reference gene *Ec*β-actin or *Lc*β-actin using the $2^{-\Delta\Delta Ct}$ method (18). The fold change in gene expression levels for each time point was calculated by comparing normalized gene expression levels in the *Lc*IFNd-stimulated and BSA-stimulated groups. All data were obtained from three independent experiments, and each analysis was performed in triplicate.

Western blots for protein expression and phosphorylation analyses

To determine the protein expression patterns and protein phosphorylation of STAT1 and STAT2 after r*Lc*IFNd induction, isolated 2×10^7 PKL cells were incubated with r*Lc*IFNd at a 250 ng/ml final concentration for 0, 15, 30, or 45 min at 28°C. PKL cells treated with control protein (Nus-tag) served as the control. For Western blots, cells were harvested and lysed in RIPA (radioimmunoprecipitation assay) buffer (P0013K, Beyotime). To detect the STAT1 and STAT2 expression patterns and STAT1 phosphorylation, cell lysates were separated using 8% SDS-PAGE gels and blotted onto a polyvinylidene difluoride membrane for immunoblotting with the following Abs: rabbit anti-STAT1 (9172S, CST), rabbit anti-STAT2 (4594S, CST), and rabbit anti–p-STAT1 (7649S, CST) as primary Abs and goat anti-rabbit IgG (H+L) HRP (S0001, Affinity Biosciences) as the secondary Ab. For STAT2 phosphorylation, the

cell lysates were separated using 8% Phos-tag SDS-PAGE gels (304-93526, Wako) and blotted onto polyvinylidene difluoride membranes for Western blot analysis with the rabbit anti-STAT2 as the primary Ab and the goat anti-rabbit IgG (H+L) HRP (S0001, Affinity Biosciences) as the secondary Ab. The methods used for Western blots are detailed in Mu et al. (39).

Blocking assays

To determine whether *Lc*IFNd activates the JAK-STAT signaling pathway via a receptor-binding mechanism, *Lc*CRFB1 and/or *Lc*CRFB5 blocking assays were performed using rabbit anti–*Lc*CRFB1-Ex and rabbit anti–*Lc*CRFB5-Ex pAbs. PKL cells (1×10^6 cells per well) were plated in six-well plates and incubated with anti–*Lc*CRFB1-Ex and/or anti-*Lc*CRFB5 pAbs for 3 h. After changing the medium, the cells were treated with r*Lc*IFNd at a final concentration of 250 ng/ml. After 12 h of *Lc*IFNd treatment, the PKL cells were harvested for total RNA extraction and reverse transcribed into cDNA. Expression levels of the key signaling molecules (JAK1, IRF9, STAT1, and STAT2) and antiviral genes (MxA, PKR, and viperin) were determined by real-time PCR, and levels of STAT1 and STAT2 phosphorylation were determined by Western blots as above. PKL cells treated with nonspecific rabbit Abs were used as controls.

Statistical analysis

Statistical analysis was performed using the IBM SPSS Statistics 2.0 software platform with one-way ANOVA, with "$p < 0.05$" or "$p < 0.01$" being considered statistically significant.

Results

Lc*CRFB1 and* Lc*CRFB5 are potential functional receptors of* Lc*IFNd*

Previous studies have shown that *Lc*IFNd can upregulate the transcription level of the antiviral gene MxA (25). To investigate which *Lc*CRFB acts as the receptor for *Lc*IFNd, we separately cloned genes encoding five *L. crocea* CRFB family members, which belong to the orthologs of mammalian type I IFN receptors and contain extracellular and intracellular domains (CRFB1, CRFB2, CRFB3, CRFB4, and CRFB5) into the pcDNA3.1 vector. EPC cells were transfected with a Dual-Luciferase reporter plasmid containing the promoter region of the MxA gene and one of the recombinant pcDNA3.1 vectors carrying *L. crocea* CRFB1, CRFB2, CRFB3, CRFB4, or CRFB5. The cells were then stimulated with r*Lc*IFNd for 24 h, followed by measurement of luciferase activity. Transfection of CRFB1 or CRFB5 significantly increased MxA response, whereas simultaneous transfection with CRFB1 and CRFB5 led to a >2-fold increase in MxA response compared with cells transfected with the control vector (Fig. 1A), suggesting that both CRFB1 and CRFB5 receptors may respond to *Lc*IFNd stimulation.

To characterize interaction between *Lc*IFNd and the extracellular region of *Lc*CRFB1 and *Lc*CRFB5, we next performed GST pull-down assays. The results showed that both *Lc*CRFB1-Ex and *Lc*CRFB5-Ex could be pulled down by *Lc*IFNd (Fig. 1B). Using ITC, we determined that *Lc*CRFB1-Ex and *Lc*IFNd interact with a K_d of 1.28 μM and stoichiometric coefficient N of 1.24 (Fig. 1C). *Lc*CRFB5-Ex and *Lc*IFNd were found to interact with >6-fold greater affinity (K_d = 203.80 nM, N = 1.14) (Fig. 1D). Meanwhile no interaction between *Lc*CRFB1-Ex and *Lc*CRFB5-Ex was observed (Supplemental Fig. 1C). These results suggest that *Lc*IFNd can interact with both *Lc*CRFB1 and *Lc*CRFB5 and may signal via a receptor complex composed of *Lc*CRFB1 and *Lc*CRFB5.

Crystal structure of Lc*IFNd*

To gain better understanding of *Lc*IFNd at the molecular level, we determined its crystal structure at a 1.49-Å resolution. The crystal belongs to the primitive P1 21 1 space group with one molecule per asymmetric unit. Details of diffraction data, phasing, and refinement statistics are listed in Table I. *Lc*IFNd has a characteristic type I IFN architecture with six α helices, designated A–F, of which helix B is the shortest. A single disulfide bridge C3-105 connecting helix A to helix D is visible in the structure. The helix F of *Lc*IFNd is long and straight, which is the hallmark of type I IFNs (Fig. 2A). Comparing the structure of *Lc*IFNd to available structures of type I IFNs suggests remarkable similarities with other reported fish (Fig. 2B, top panel) and mammalian type I IFNs (Fig. 2B, bottom panel). A major structural distinction is the AB loop, on which no helical structure is present. Such AB loop structure is consistent with zIFN-φ1, *Ci*IFNa, and mouse IFN-β (mIFN-β) (Fig. 2C, left panel), but different from *Lc*IFNi, zIFN-φ2, human IFN (hIFN)-α2, hIFN-ω, and hIFN-β (Fig. 2C, right panel).

Given that *Lc*IFNd contains two cysteines (C1 and C3) (Fig. 2D), it can be classified as a member of the group I of teleost type I IFNs. We compared the reported structures of fish type I IFNs and found that the C1/C3 conserved cysteine pair can form a disulfide bond linking helix A to helix D in all of the structures (Fig. 2E). Mutating either of the two cysteines resulted in low protein expression levels and significantly reduced the melting temperature value of the mutant protein (Supplemental Fig. 1D), suggesting that the disulfide bond is indispensable for the folding and stability of *Lc*IFNd.

The helix E on Lc*IFNd is a key region involved in* Lc*CRFB1 binding*

To investigate the *Lc*IFNd–*Lc*CRFB1 and *Lc*IFNd–*Lc*CRFB5 interactions in more detail, we next carried out NMR analysis. We first performed ^{1}H, ^{13}C, and ^{15}N backbone and side-chain resonance assignments of the *Lc*IFNd (residues 21–185) by using heteronuclear multidimensional NMR spectroscopy. Backbone and side-chain resonances of the *Lc*IFNd were assigned based on the recorded heteronuclear two-dimensional/three-dimensional NMR spectra (Supplemental Fig. 1E). In total, ~70.7% of the ^{1}H and ^{15}N resonances of all nonproline residues were assigned unambiguously. For clarity, distribution patterns with the assigned or the unassigned residues are shown in the structure and sequences of *Lc*IFNd (Supplemental Fig. 1F).

To identify specific amino acids in *Lc*IFNd involved in the interaction with *Lc*CRFB1, *Lc*CRFB1-Ex protein samples were titrated with deuterated *Lc*IFNd by NMR titrations. Superimposition of the two-dimensional ^{1}H-^{15}N-HSQC spectrum of *Lc*IFNd and *Lc*IFNd+*Lc*CRFB1-Ex showed that the *Lc*CRFB1-Ex induced significant structural changes in the *Lc*IFNd (Fig. 3A), indicating formation of the *Lc*CRFB1-Ex–*Lc*IFNd complex. In contrast, few amino acids underwent significant chemical shifts upon titration of the *Lc*CRFB5-Ex with *Lc*IFNd (Fig. 3B), indicating that chemical exchange processes between *Lc*CRFB5-Ex and *Lc*IFNd are in the slow-exchange regimen. We also observed that chemical shift perturbations for *Lc*IFNd mainly localized to residues within the 112–136 region (Fig. 3Ca). In particular, the residues shifted mainly in helix E (residues 114–133) and E–F loop (residues 134–136) (Fig. 3Cb), with addition of several scattered residues, such as A42, K59, and A138, and R144 (Fig. 3Ca).

Considering that the aforementioned chemical shift perturbation occurred upon adding *Lc*CRFB1-Ex to *Lc*IFNd, we hypothesized that the shifted residues may be involved in *Lc*CRFB1 binding. To verify our hypothesis, we performed pull-down assays with *Lc*IFNd in which shifted residues were mutated to alanine. The shifted residues were selected based on their side chain properties or spatial distribution (Fig. 3Cc), which resulted in preparation of nine single-residue mutations in helix E (K113A, K114A, H119A, K123A, R124A, H128A, K131A, K132A, and H135A) and a multiple-residue mutation in which all nine residues were mutated to alanine (referred to as MαE). The results of pull-down assays showed that mutants MαE, K113A, K114, H119, K123A, R124A, H128A, and H135A significantly reduce the ability of *Lc*IFNd to bind *Lc*CRFB1-Ex (Fig. 3D). These findings indicate that helix E of *Lc*IFNd

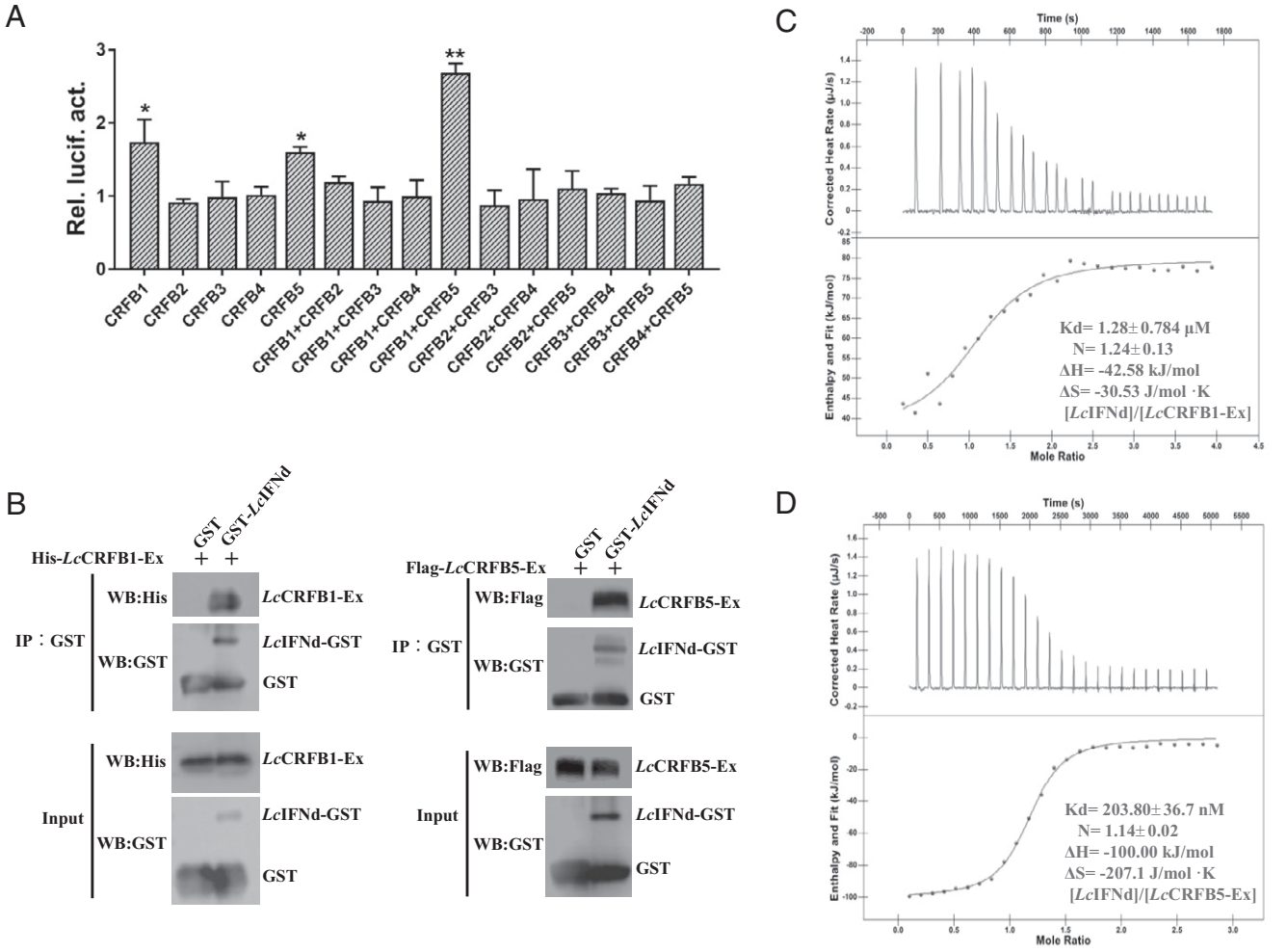

FIGURE 1. *Lc*CRFB1 and *Lc*CRFB5 are potential functional receptors of *Lc*IFNd. (**A**) Levels of luciferase activity in EPC cells transfected with vectors expressing different CRFB receptors upon stimulation with r*Lc*IFNd and control protein (Nus-tag). The Dual-Luciferase reporter plasmid pGL3-Basic contained the promoter region of the antiviral IFN-stimulated gene MxA from *L. crocea*. (**B**) Results of pull-down assays examining the interactions between *Lc*IFNd and extracellular regions of *Lc*CRFB1 and *Lc*CRFB5. (**C** and **D**) ITC binding curves for (C) titration of *Lc*IFNd (100 μM) into *Lc*CRFB1-Ex (30 μM) and (D) titration of *Lc*IFNd (60 μM) into *Lc*CRFB5-Ex (50 μM). The K_d and stoichiometry (N) values are expressed as mean ± SD, and all ITC experiments were repeated at least three times. Bars represent the means of three independent experiments ± SD. All experiments were performed in triplicate. $^*p < 0.05$, $^{**}p < 0.01$.

(particularly residues K113, K114, H119, K123, R124, H128, and H135) is the key structural element involved in *Lc*CRFB1 binding.

The interface formed by helices C–D–E of Lc*IFNd mediates binding to* Lc*CRFB1*

Although the aforementioned results of NMR titration and pull-down assays show that the helix E of *Lc*IFNd is crucial for *Lc*CRFB1 binding, we speculate that the binding interface is likely to encompass additional regions of *Lc*IFNd. Moreover, NMR titration with *Lc*IFNd and *Lc*CRFB5-Ex did not produce any significant chemical shifts in *Lc*IFNd, leaving the interaction uncharacterized. Therefore, to further characterize the interactions between *Lc*IFNd and *Lc*CRFB1 and *Lc*CRFB5, we predicted the structures of *Lc*CRFB1-Ex and *Lc*CRFB5-Ex using AlphaFold v2.0 and constructed structural models of *Lc*IFNd–*Lc*CRFB1-Ex and *Lc*IFNd–*Lc*CRFB5-Ex complexes (described in *Materials and Methods*). The structural models strongly suggest the involvement of the "elbow" regions formed between two bent FNIII domains (D1 and D2) of *Lc*CRFB1-Ex and *Lc*CRFB5-Ex in *Lc*IFNd recognition (Supplemental Fig. 1G, 1H) (40, 41). This subsection focuses on the analysis of *Lc*IFNd–*Lc*CRFB1 interactions, whereas the *Lc*IFNd–*Lc*CRFB5-Ex interactions are analyzed in detail in the following subsection.

Electrostatic surface potential analysis showed that the surface of helix E in *Lc*IFNd is formed mainly by positively charged amino acids, which is in line with data from the NMR titration experiments (Fig. 4A, left panel). Conversely, parts of helix C, loop CD, and helix D (residues E67, E68, E74, E75, D76, E85, and E89) form a continuous negatively charged surface area (Fig. 4A, left panel). The surface charge on one face of *Lc*IFNd is thus distributed to form a positively charged region (PCR) and a negatively charged region (NCR). Notably, we also found that the elbow region of *Lc*CRFB1-Ex contains prominent positively and negatively charged surfaces (Fig. 4A, right panel). These observations suggest that binding of *Lc*IFNd to *Lc*CRFB1-Ex may rely on paired interactions with the surfaces of opposite charge on *Lc*CRFB1-Ex, which would form two binding pockets (site 1 and site 2) (Fig. 4B, 4C). In site 1, the intermolecular contacts are established between the helix E of *Lc*IFNd and the D2 domain of *Lc*CRFB1-Ex, with salt bridges or polar interactions formed between residue pairs $K113_{IFNd}$-$D125_{CRFB1}$, $K114_{IFNd}$-$E116_{CRFB1}$, $H119_{IFNd}$-$E122_{CRFB1}$, $K123_{IFNd}$-$D124_{CRFB1}$, $H128_{IFNd}$-$D153_{CRFB1}$, and $H135_{IFNd}$-$E152_{CRFB1}$ (Fig. 4Ca). In site 2,

Table I. Crystallographic data collection and structure refinement statistics

Dataset	*Lc*IFNd
Data collection	
Beamline	BL-02U1, SSRF
Wavelength (Å)	0.97918
Resolution range[a,b]	37.22–1.49 (1.543–1.49)
Space group	P 1 21 1
Cell dimensions	
a, *b*, *c* (Å)	40.378, 38.813, 51.091
α, β, γ (°)	90.00, 112.817, 90.00
Total reflections	45,866 (4,719)
Unique reflections	23,089 (2,374)
Multiplicity	2.0 (2.0)
Completeness (%)	95.80 (98.67)
Mean I/σ I	16.59 (2.41)
R_{merge}	0.02326 (0.2676)
R_{meas}	0.03289 (0.3784)
R_{pim}	0.02326 (0.2676)
CC1/2	0.999 (0.888)
Refinement	
Reflections used in refinement	23,060 (2,372)
Reflections used for R_{free}	1089 (126)
R_{work}	0.1746 (0.2301)
R_{free}	0.2242 (0.2824)
Wilson B factor (Å^2)	18.98
Number of nonhydrogen atoms	1357
Macromolecules	1206
Protein residues	150
RMS (bonds)	0.017
RMS (angles)	1.99
Ramachandran favored (%)	99.32
Ramachandran allowed (%)	0.68
Ramachandran outliers (%)	0.00
Rotamer outliers (%)	1.53
Clashscore	5.49
Average B factor (Å^2)	27.52

CC1/2, Pearson correlation coefficient between two randomly selected halves of the dataset; mean I/σ I, mean average intensity/average intensity error; SSRF, Shanghai Synchrotron Radiation Facility.

[a]One crystal sample was used for structure determination. Values in parentheses are for the highest-resolution shell.

[b]CC1/2 in the highest resolution shell was statistically significant at the 0.1% level.

the intermolecular contacts are established between the helices C–D of *Lc*IFNd and the D1 domain of *Lc*CRFB1-Ex, with salt bridges or polar interactions formed between residue pairs $E67_{IFNd}$-$K45_{CRFB1}$, $E74_{IFNd}$-$R37_{CRFB1}$, $E74_{IFNd}$-$K39_{CRFB1}$, $D76_{IFNd}$-$R63_{CRFB1}$, $E89_{IFNd}$-$R40_{CRFB1}$, and $E85_{IFNd}$-$K41_{CRFB1}$ (Fig. 4Cb). Using isothermal calorimetry, we checked *Lc*IFNd mutants MαE and MαC-D (all negatively charged residues in the NCR of *Lc*IFNd substituted to alanine; more details are provided in *Materials and Methods*) for their ability to bind *Lc*CRFB1-Ex in vitro. Both mutants lost their ability to bind *Lc*CRFB1-Ex (Supplemental Fig. 1I), suggesting that helices C–D and E of *Lc*IFNd form key interfaces for binding to *Lc*CRFB1. Noted that although both *Lc*IFNd and hIFN-ω interact respectively with *Lc*CRFB1-Ex and hIFNAR1 through interface formed by helices C–D and E, the amino acid residues involved in receptor binding are generally not conserved between *Lc*IFNd and hIFN-ω (Fig. 4Cc, d).

Identification of key Lc*IFNd regions and residues involved in the interaction with* Lc*CRFB5*

The crystal structure of *Lc*IFNd and the predicted structure of *Lc*CRFB5-Ex display high similarity to the structures of hIFN-ω and the hIFNAR2 extracellular region (18), respectively (Fig. 2B, bottom panel, Supplemental Fig. 1H, left). Considering these similarities, we superimposed the crystal structure of *Lc*IFNd and the predicted structure of *Lc*CRFB5-Ex with the previously reported structure of the hIFN-ω–IFNAR2 binary complex (PBD ID: 3SE4) to construct the structural model of the *Lc*IFNd–*Lc*CRFB5-Ex complex. *Lc*IFNd and *Lc*CRFB5-Ex aligned well with the hIFN-ω–IFNAR2 binary complex (Supplemental Fig. 1H, right), implying conservation of receptor binding modes. To identify the key amino acids involved in the binding of *Lc*IFNd to *Lc*CRFB5, we analyzed the charge distribution at the predicted *Lc*IFNd–*Lc*CRFB5-Ex interaction interface. The binding interface between the two proteins encompasses predominantly hydrophobic interactions, with the addition of some polar interactions (Fig. 5A, left and middle panels). Two main intermolecular interface sites can be observed in the predicted model of the *Lc*IFNd–*Lc*CRFB5-Ex complex (Fig. 5B). In the first site, a large hydrophobic pocket is formed between residues L18, F43, and M152 of *Lc*IFNd and P51, I77, V79, and L95 of *Lc*CRFB5-Ex. In addition, residues E33 and D34 of *Lc*IFNd and residues R81 and H90 of *Lc*CRFB5-Ex may form polar interactions (Fig. 5Ba). The second interacting site mainly comprises polar interactions or salt bridges between residues R11, E15, and D155 of *Lc*IFNd and R140, and E141 of *Lc*CRFB5-Ex, respectively (Fig. 5Bb). Through further comparison, we found that the amino acid residues F29, L32, and R35 of hIFN-ω involved in receptor binding via the AB loop are different from these amino acids, E33, D34, and D39 of *Lc*IFNd (Fig. 5Bc). Similarly, the hydrophobic region consisting of L18, F43, and M150 in *Lc*IFNd is located in the same region as the hydrophobic interaction region consisting of L17, V18, M151, F155, and L156 in hIFN-ω. In addition, L18 of *Lc*IFNd and L17 of hIFN-ω are highly conserved in this region (Fig. 5Bd). Results of pull-down assays demonstrated that GST-tagged *Lc*IFNd mutants L18A and F43A almost entirely abolished binding to Flag-tagged *Lc*CRFB5-Ex, whereas mutants E15A, K145A, M152A, and D155A could weaken the binding (Fig. 5C). Altogether, our results show that the residues E15, L18, F43, K145A, M152A, and D155 of *Lc*IFNd are important for binding to the extracellular region of *Lc*CRFB5.

Lc*IFNd activates JAK-STAT signaling*

Previous studies have demonstrated that *L. crocea* possesses an evolutionarily conserved JAK-STAT pathway that is likely to perform regulatory functions similar to those in higher vertebrates (18). To investigate *Lc*IFNd-mediated signal transduction, we stimulated PKL cells with r*Lc*IFNd and monitored the activation of the JAK-STAT pathway. The mRNA expression levels of JAK1, IRF9, STAT1, and STAT2 (Fig. 6Aa) and IFN-stimulated antiviral genes MxA, PKR, and viperin (Fig. 6Ab) were significantly increased at 6 or 12 h after *Lc*IFNd stimulation. Meanwhile, r*Lc*IFNd significantly increased phosphorylation levels of both STAT1 (Fig. 6B) and STAT2 (Fig. 6C). The antiviral activity of r*Lc*IFNd was examined using the SIGV-infected GS cells model as described previously (25). We found that pretreatment of GS cells with r*Lc*IFNd 2 h prior to SIGV infection resulted in significant inhibition of CPE compared with the control cells (Fig. 6Da), which was accompanied by a reduced expression of viral genes at 12 or 24 h (Fig. 6Db). These results showed that *Lc*IFNd activates the JAK-STAT signaling pathway in a conserved manner, as found in higher vertebrates, leading to transcription of IFN-stimulated antiviral genes such as MxA, PKR, and viperin.

Lc*IFNd signaling requires* Lc*CRFB1 and* Lc*CRFB5*

The findings of this study have demonstrated that *Lc*CRFB1 and *Lc*CRFB5 serve as receptors of *Lc*IFNd. To further verify whether *Lc*CRFB1 and *Lc*CRFB5 are required for *Lc*IFNd signaling, we prepared anti–*Lc*CRFB1-Ex and anti–*Lc*CRFB5-Ex pAbs and performed an Ab blockade assay. Anti–*Lc*CRFB1-Ex pAb specificity was validated by Western blot and immunofluorescence assays (Fig. 7A), and anti–*Lc*CRFB5-Ex pAb specificity was validated as described previously (18). PKL cells stimulated with r*Lc*IFNd in the

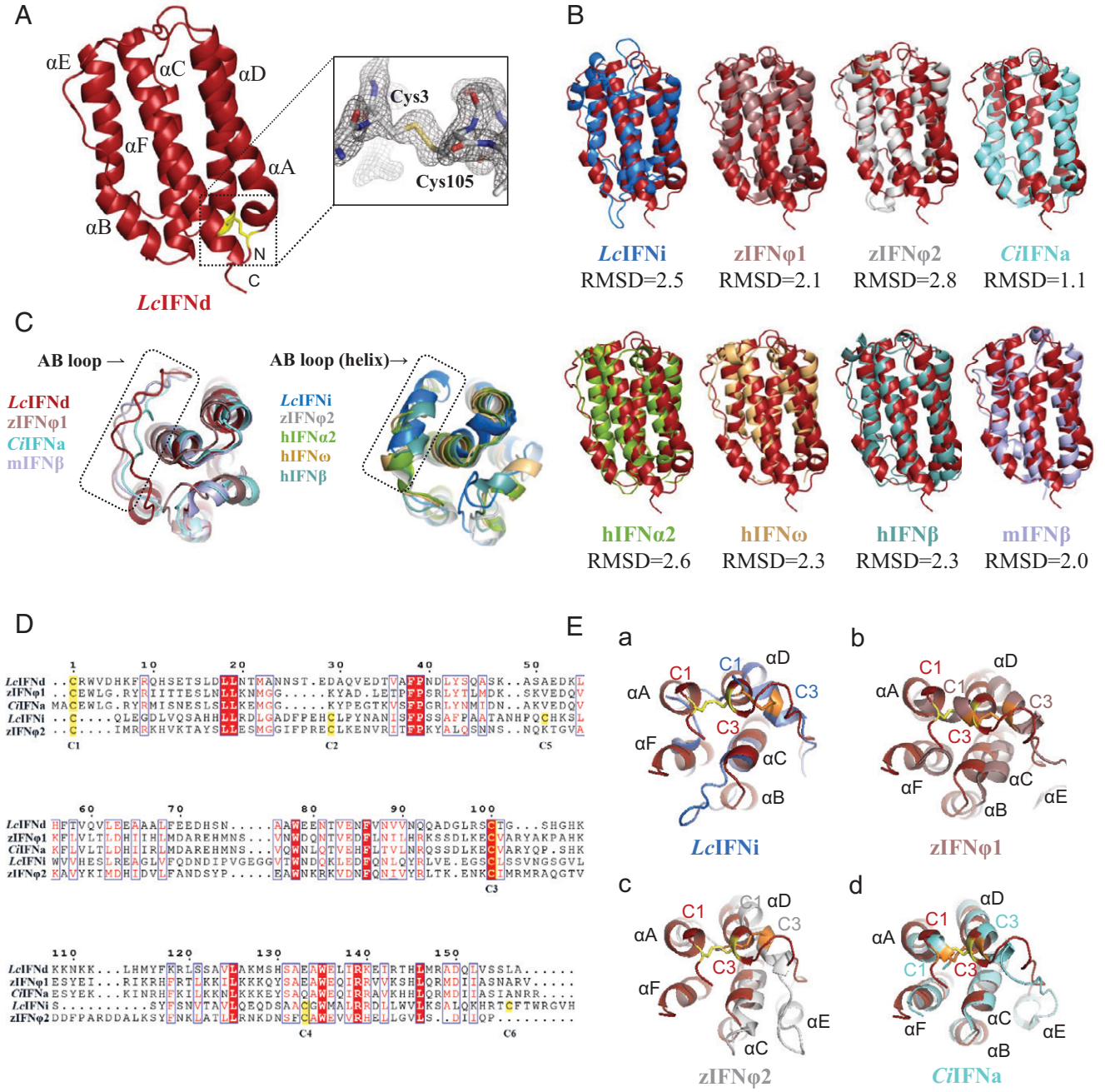

FIGURE 2. Structure analysis of *Lc*IFNd. (**A**) Structure of *Lc*IFNd in cartoon representation. Secondary structural elements are labeled A–F. The N terminus and C terminus are indicated with N and C, respectively. One disulfide bond is colored yellow and shown in detail with surrounding residues as 2Fo-Fc electron density maps contoured at the 1.0 σ level. (**B**) Superimposition of *Lc*IFNd (firebrick) with *Lc*IFNi (PDB ID: 7WZ5, marine), zIFN-φ1 (PDB ID: 3PIV, dark violet), zIFN-φ2 (PDB ID: 3PIW, gray 90), *Ci*IFNa (PDB ID: 7WKH, aquamarine), hIFN-α2 (PDB ID: 1RH2, split-pea), hIFN-ω (PDB ID: 3SE4, tv-orange), hIFN-β (PDB ID: 1AU1, cyan-light teal), and mIFN-β (PDB ID: 1IFA, light orange). All structures were superimposed in PyMOL using the "align" command. (**C**) Left, Superimposition of *Lc*IFNd, zIFN-φ1, *Ci*IFNa, and mIFN-β. Right, Superimposition of *Lc*IFNi, zIFN-φ2, hIFN-α2, hIFN-ω, and hIFN-β. (**D**) Multiple alignment of mature peptide sequence of *Lc*IFNd with other fish type I IFNs whose crystal structures have been resolved. The conserved cysteine residues involved in forming intramolecular disulfide bonds are indicated by paired lines (C1–C3, C2–C4, and C5–C6) and highlighted in yellow. The cysteine residues C1 and C3 are marked with a star (★)below the alignment. (**E**) Representation of the C1–C3 disulfide bond in *Lc*IFNd (yellow) superimposed with *Lc*IFNi (**a**, orange), zIFN-φ1 (**b**, orange), zIFN-φ2 (**c**, orange), and *Ci*IFNa (**d**, orange).

presence of anti–*Lc*CRFB1-Ex, anti–*Lc*CRFB5-Ex, or both pAbs exhibited a dramatic decrease in expression levels of JAK1, IRF9, STAT1, and STAT2 (Fig. 7B), as well as MxA, PKR, and viperin (Fig. 7C). Similarly, the phosphorylation of STAT1 and STAT2 were significantly weakened by blocking *Lc*CRFB1 and *Lc*CRFB5 (Fig. 7D). These results confirm that both *Lc*CRFB1 and *Lc*CRFB5 are required for *Lc*IFNd signaling, and blocking either of the receptor subunits is sufficient to inhibit the activation of JAK-STAT signaling pathway, which in turn inhibit the transcription of ISGs (Fig. 8).

To investigate the importance of the aforementioned key *Lc*IFNd residues involved in receptor binding on *Lc*IFNd signaling, PKL cells were stimulated with the relevant *Lc*IFNd mutants, and expression levels of key signaling molecules (JAK1 and STAT1) and

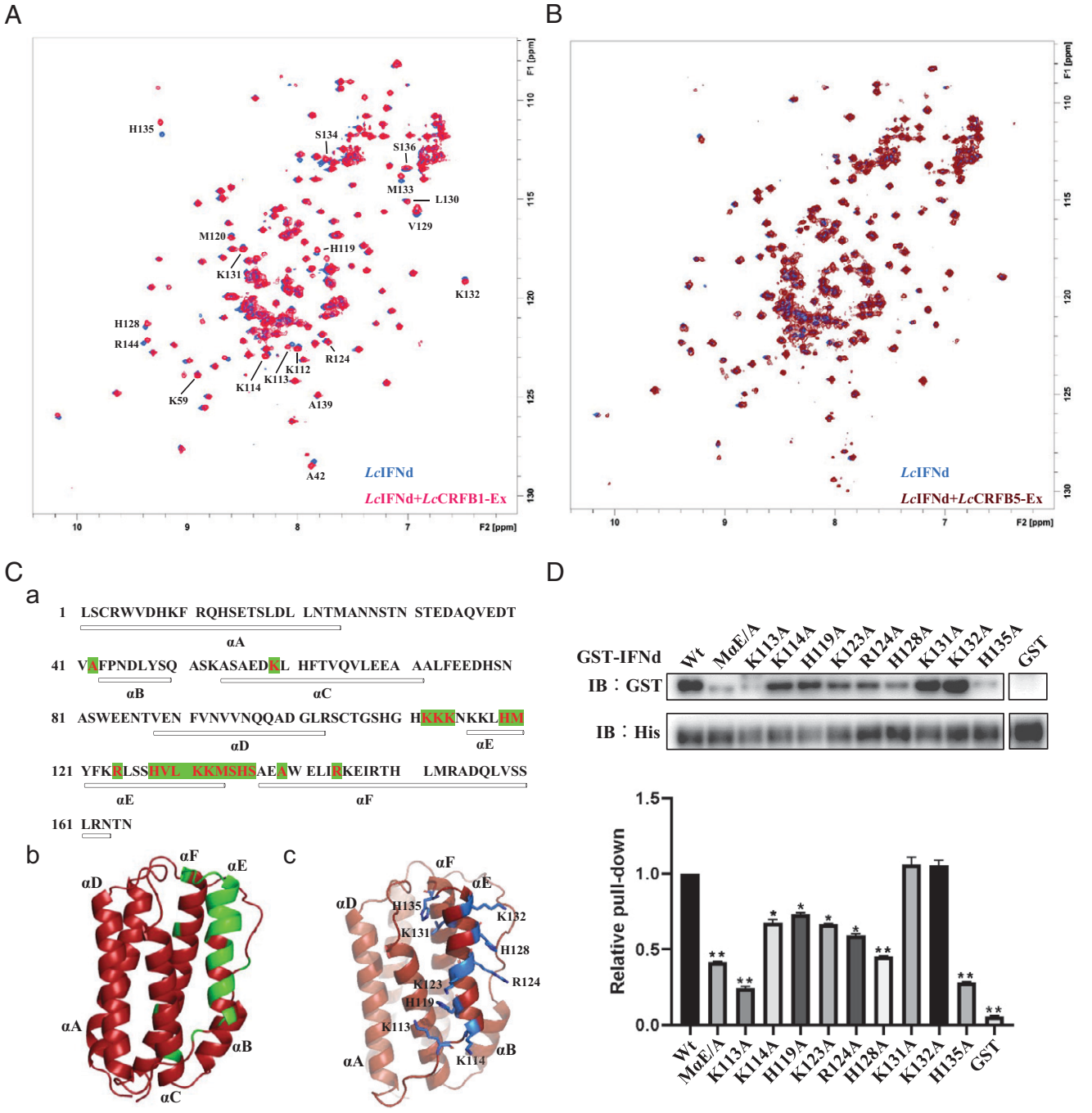

FIGURE 3. The helix E on *Lc*IFNd is a key region involved in *Lc*CRFB1 binding. (**A**) ^{1}H-^{15}N HSQC spectra of *Lc*IFNd (blue) and *Lc*IFNd in complex with *Lc*CRFB1-Ex (pink). Amino acids exhibiting chemical shifts are labeled with their name and residue number. (**B**) ^{1}H-^{15}N HSQC spectra of *Lc*IFNd (blue) and *Lc*IFNd in complex with *Lc*CRFB5-Ex (wine red). Note that few amino acids underwent significant chemical shifts. (**C**) **a**, Amino acid sequence of *Lc*IFNd. Rectangles underneath the sequence represent α helices A–F. Amino acid residues with chemical shifts are highlighted in green. **b**, Structure of *Lc*IFNd with the *Lc*CRFB1-binding region as identified by NMR titration (as in **A**) colored green. **c**, Structure of *Lc*IFNd with side chains of positively charged residues K113, K114, H119, K123, R124, H128, K131, K132, and H135 on α helix E shows as blue sticks. (**D**) Results of pull-down assays examining binding between His-tagged *Lc*CRFB1-Ex and GST-tagged *Lc*IFNd mutant variants. Histograms represent the pull-down ability based on band intensities relative to the value of wild-type GST-*Lc*IFNd pulled down by Flag-*Lc*CRFB1-Ex, which was defined as 1. The band intensities were quantified using ImageJ software. Bars represent the means of three independent experiments ± SD. All experiments were performed in triplicate. $*p < 0.05$, $**p < 0.01$.

antiviral effectors (MxA and PKR) were quantified at 6 h poststimulation. Compared to wild-type *Lc*IFNd, the mRNA levels of the four genes were significantly reduced when PKL cells were stimulated with the *Lc*CRFB1-Ex–binding mutants MαE, K113A, H119A, K123A, R124A, H128A, H135A, and MαC-D (Supplemental Fig. 2A). Similarly, the mRNA levels of the same genes were significantly reduced when stimulating cells with *Lc*CRFB5-Ex–binding mutants E15A, L18A, F43A, K145A, M152A, and D155A (Supplemental Fig. 2B). Taken together with the results of pull-down assays and the *Lc*IFNd mutants described above (Figs. 3D, 5C), these data suggest that the *Lc*IFNd residues K113, H119, K123, R124, H128, and H135 are critical for binding to *Lc*CRFB1, and that *Lc*IFNd residues

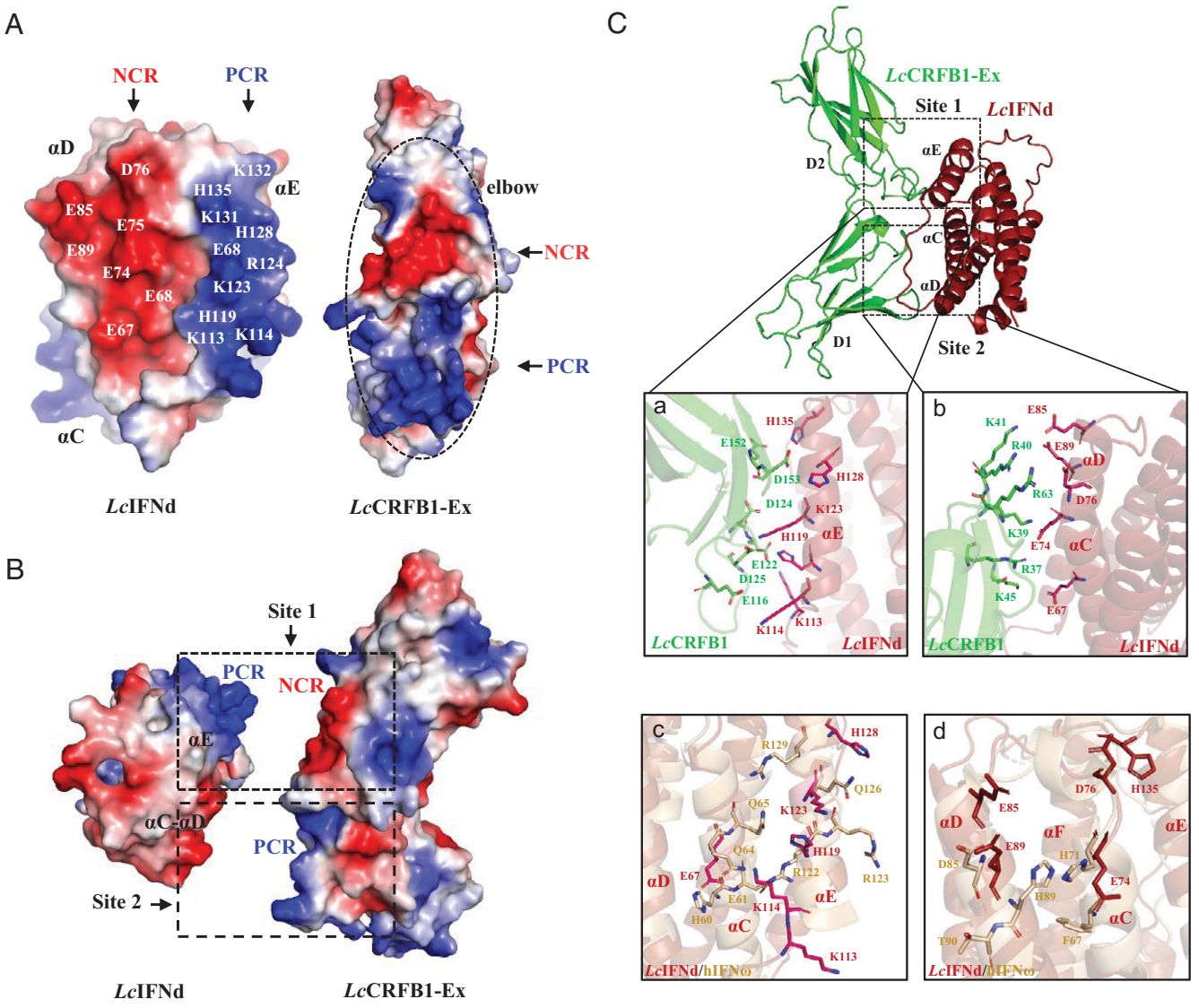

FIGURE 4. The helix C–D–E interface of *Lc*IFNd is involved in *Lc*CRFB1 binding. (**A**) Left, Surface charge distribution of the helix C–D–E interface of *Lc*IFNd. The negatively charged region (NCR) and the positively charged region (PCR) on the interface are indicated in red and blue, respectively. Residues predicted to be involved in interaction with *Lc*CRFB1 are labeled. Right, Surface charge distribution of *Lc*CRFB1-Ex. (**B**) Surface charge distribution of binding model between *Lc*IFNd and *Lc*CRFB1-Ex. Site 1 represents the binding region between the PCR of *Lc*IFNd and the NCR of *Lc*CRFB1-Ex, whereas site 2 represents the binding region between the NCR of *Lc*IFNd and the PCR of *Lc*CRFB1-Ex. (**C**) Predicted structural model of the *Lc*IFNd–*Lc*CRFB1-Ex complex with relative locations of the two interacting sites. The first (**a**) and the second (**b**) interacting sites are shown in a detailed view. Interacting residues of *Lc*IFNd and *Lc*CRFB1 are colored firebrick and green, respectively. A detailed view of superimposed *Lc*IFNd and hIFN-ω regions mediating interactions with *Lc*CRFB1 and hIFNAR1 (**c** and **d**, respectively) is shown. Interacting residues are shown as sticks and colored firebrick and light orange, respectively.

E15, L18, F43, K145, M152, and D155 are critical for binding to *Lc*CRFB5.

Discussion

In mammals, type I IFNs are the main orchestrators of the antiviral innate immune response. All 16 human type I IFNs initiate signaling by binding to the same receptors composed of the IFNAR1 and IFNAR2 subunits. In zebrafish and pufferfish, however, genome-wide sequence analyses demonstrated the presence of at least 17 CRFB members (19, 42). Recent studies on type I IFN receptors in teleost fish have focused on signaling through CRFB1, CRFB2, and CRFB5. Thus far, research suggests that fish group I IFNs signal through the receptor complex consisting of CRFB1–CRFB5 and that fish group II IFNs signal through CRFB2–CRFB5 (18, 20). However, *Ci*IFNa in grass carp (a group I IFN) was found to signal through CRFB1, CRFB2, and CRFB5 (23). Here, our findings unambiguously demonstrate that the IFNd from *L. crocea*, a group I IFN, binds the CRFB1/CRFB5 receptor pair (Fig. 1A, 1B).

The ITC results in this study show that *Lc*IFNd binds *Lc*CRFB5-Ex with a higher affinity (K_d = 203.80 nM) than *Lc*CRFB1-Ex (K_d = 1.28 μM) (Fig. 1C, 1D). Furthermore, we did not observe significant ^{1}H and ^{15}N chemical shifts in *Lc*IFNd upon *Lc*CRFB5-Ex titration (Fig. 3B), indicating that *Lc*CRFB5-Ex binding to *Lc*IFNd is in a slow exchange on the NMR time scale. These findings are also in agreement with our previous observation in *L. crocea* where *Lc*CRFB5 is the higher affinity receptor (K_d = 74.64 nM) than *Lc*CRFB2 (K_d = 996.90 nM) for *Lc*IFNi (18). The grass carp IFNa also appears to have a higher binding affinity for CRFB5 than for CRFB1 and CRFB2 (23), further suggesting that CRFB5 may act as a higher affinity receptor for teleost type I IFNs, whereas CRFB1

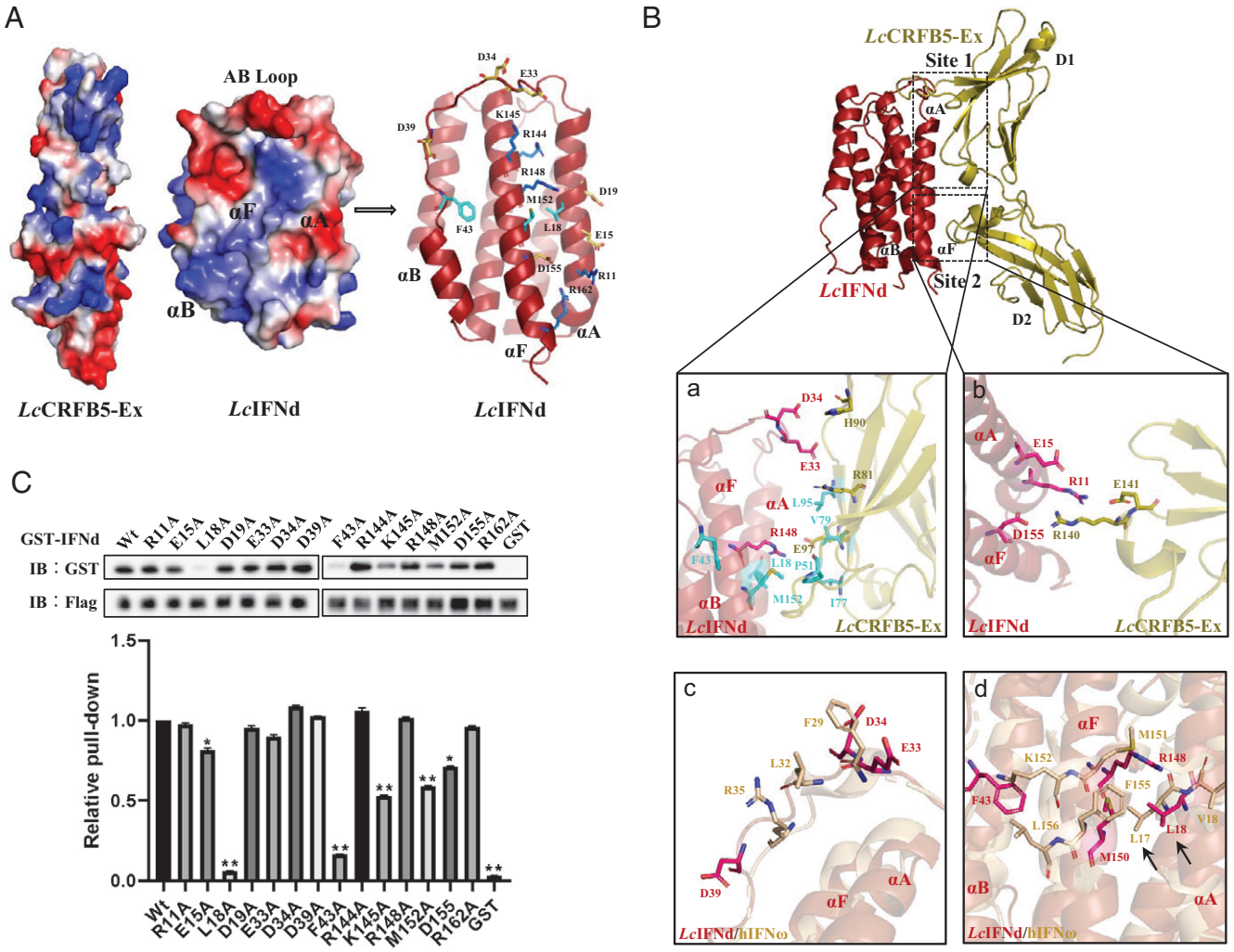

FIGURE 5. Identification of key *Lc*IFNd regions and residues involved in the interaction with *Lc*CRFB5. (**A**) Left, Surface charge distribution of *Lc*CRFB5-Ex. Middle, Surface charge distribution of the helix A–B–F interface of *Lc*IFNd. Right, *Lc*IFNd residues predicted to be involved in interaction with *Lc*CRFB5 are labeled in the structure of *Lc*IFNd. Positively charged, hydrophobic, and negatively charged residues are shown as blue, aquamarine, and yellow sticks, respectively. (**B**) Predicted structural model of the *Lc*IFNd–*Lc*CRFB5-Ex complex with relative locations of the two interacting sites. The first (**a**) and the second (**b**) interacting sites are shown in a detailed view. Interacting residues of *Lc*IFNd and *Lc*CRFB5 are colored firebrick and olive, respectively. A detailed view of superimposed *Lc*IFNd and hIFN-ω regions mediating interactions with *Lc*CRFB1 and hIFNAR2 (**c** and **d**, respectively) is shown. Interacting residues are shown as sticks and are colored firebrick and light orange, respectively. Residues L17 and L18 are indicated with a black arrow. (**C**) Results of pull-down assays examining binding between Flag-tagged *Lc*CRFB5-Ex and GST-tagged *Lc*IFNd and its mutant variants. Histograms represent the pull-down ability based on band intensities relative to the value of wild-type GST-*Lc*IFNd pulled down by Flag-*Lc*CRFB5-Ex, which was defined as 1. The band intensities were quantified using ImageJ software. Bars represent the means of three independent experiments ± SD. All experiments were performed in triplicate. $*p < 0.05$, $**p < 0.01$.

and CRFB2 may act as lower affinity receptors. Notably, IFNAR1, the ortholog of CRFB5 in mammals, serves as the high-affinity receptor for IFN-β in mice, but as the low-affinity receptor for IFN-β and IFN-α2 in humans (11, 43). These findings demonstrate that the affinity of type I IFN for their receptors may be rather varied among species.

Our structural data and analysis may also explain why fish group I and group II type I IFNs bind to CRFB1–CRFB5 and CRFB2–CRFB5 receptor complexes, respectively. The helical element in the AB loop, which is considered to be a key site involved in receptor interaction in group II IFNs such as *Lc*IFNi and zIFN-φ2 (14, 18), is absent in the group I IFNs *Lc*IFNd, zIFN-φ1 (24), and *Ci*IFNa (23) (Fig. 2C). Furthermore, the *Lc*CRFB5/*Lc*IFNd interface is formed by residues of the D1 and D2 subdomains of *Lc*CRFB5 and by helices A, B, and F of *Lc*IFNd, whereas the *Lc*CRFB5/*Lc*IFNi interface is formed by residues of the D1 and D2 subdomains of *Lc*CRFB5 and by helices C, D, and E in *Lc*IFNi (18). The differences in AB loop structure and the composition of the CRFB5-interacting interface could therefore play an important role in conferring affinity for different receptor complexes to fish group I and group II type I IFNs.

Recent studies have confirmed that the overall structure of fish type I IFNs is similar to that of mammalian type I IFNs (44, 45), as is the case with *Lc*IFNd reported in our study. Nevertheless, we also observed notable differences between IFNd receptor and IFN-ω receptor binding modes, including the helical domain and amino acid species. Interestingly, the region encompassing L18, F43, and M152 in *Lc*IFNd and the region encompassing L17, V18, M151, F155, and L156 in hIFN-ω form a hydrophobic pocket in corresponding locations (Fig. 5Bd). Moreover, L18 of *Lc*IFNd and L17 of hIFN-ω are fully conserved in this region (Fig. 5Bd), suggesting a certain degree of conservation of residues involved in receptor binding despite overall low sequence similarity between *Lc*IFNd and hIFN-ω.

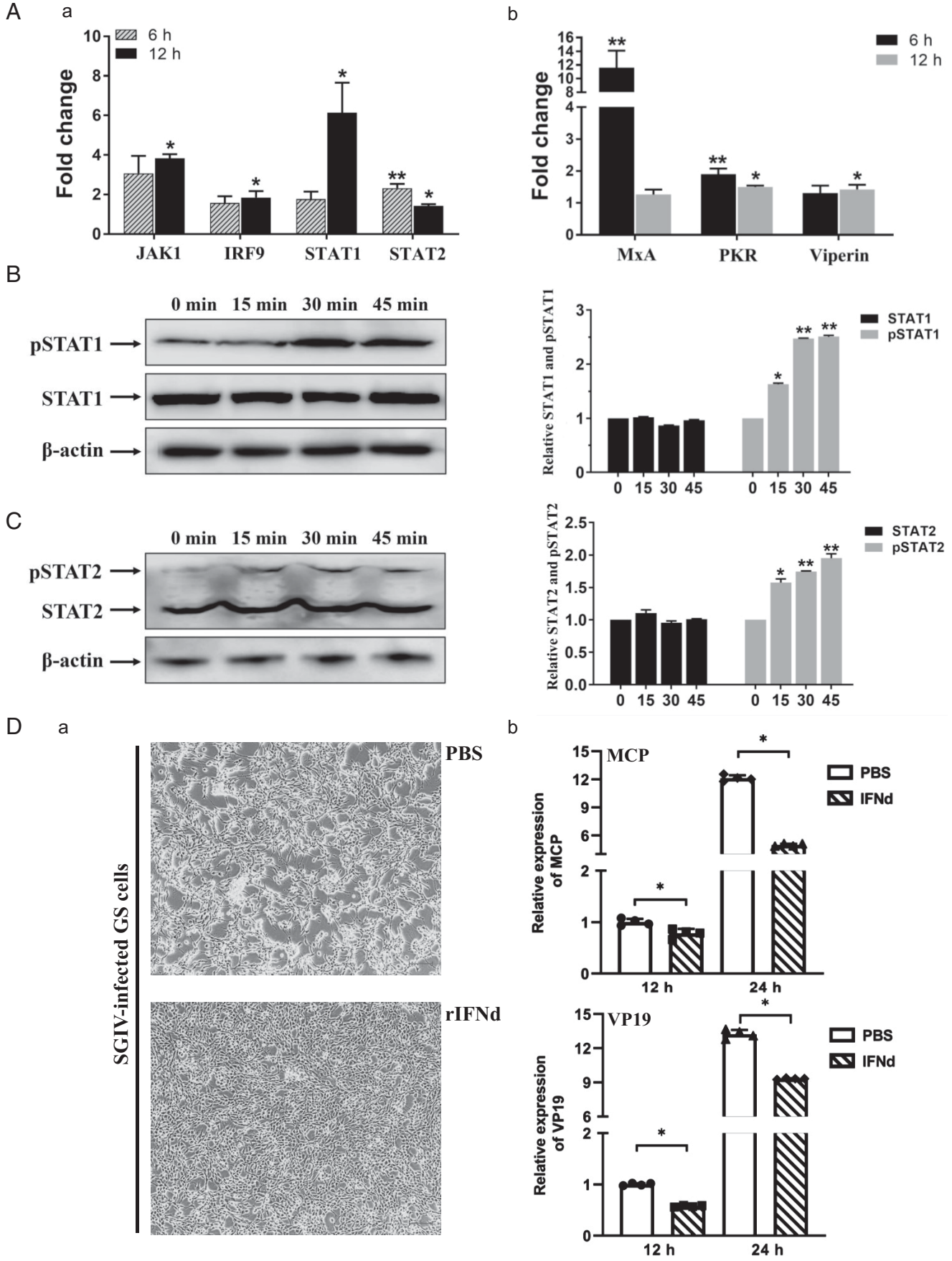

FIGURE 6. Activation of JAK-STAT signaling and antiviral activity of r*Lc*IFNd. (**A**) **a**, Expression levels of JAK-STAT pathway signaling effectors JAK1, IRF9, STAT1, and STAT2, and (**b**) IFN-stimulated antiviral genes MxA, PKR, and viperin in PKL cells determined by real-time PCR at 6 and 12 h after stimulation with r*Lc*IFNd ($n = 5$). (**B** and **C**) Left, Western blot results showing STAT1 and STAT2 expression and *(Figure legend continues)*

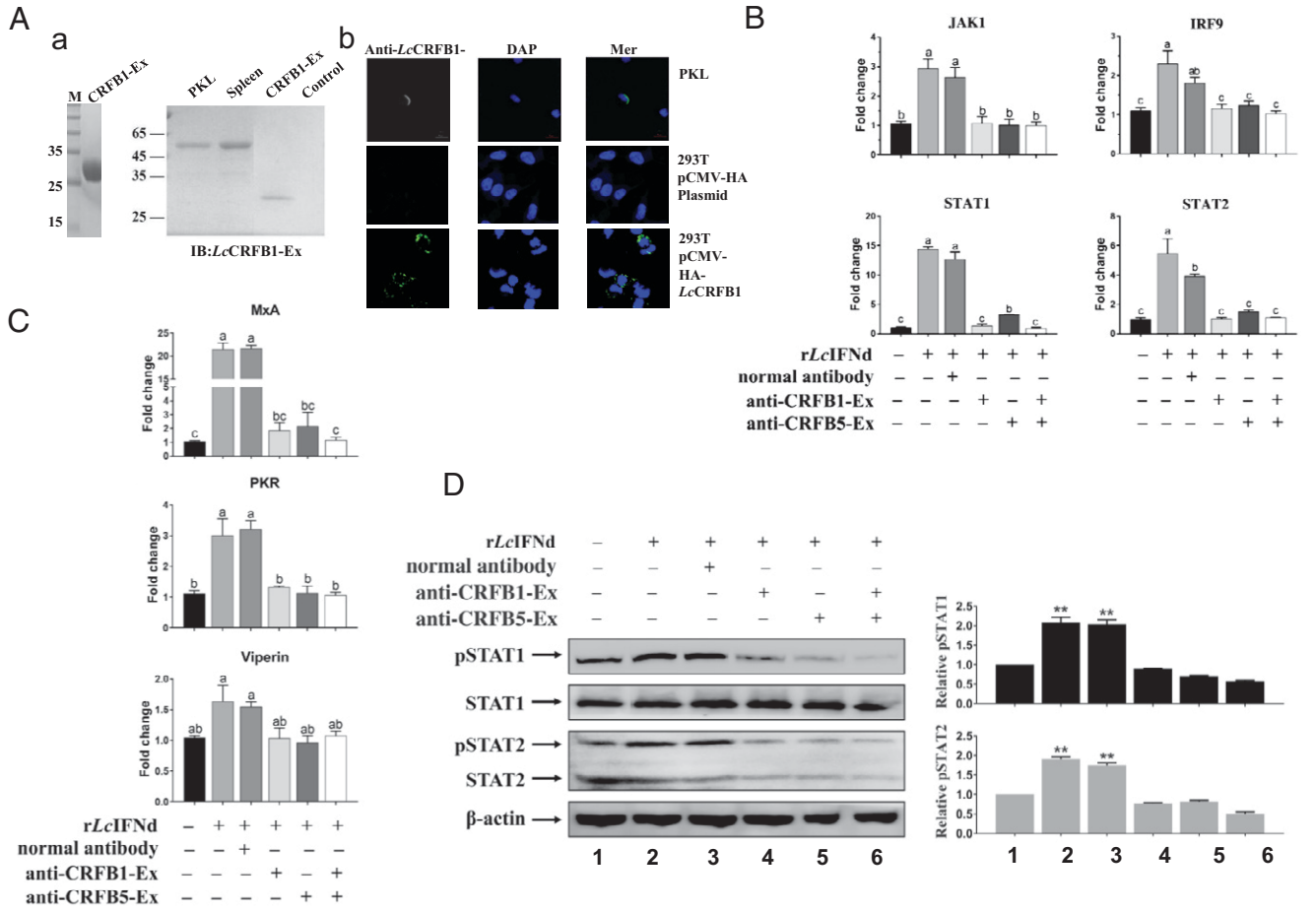

FIGURE 7. *Lc*CRFB1 and *Lc*CRFB5 receptor blockade impairs *Lc*IFNd signal transduction. (**A**) **a**, Left, SDS-PAGE gel showing purified r*Lc*CRFB1-Ex. Right, Detection of endogenous full-length *Lc*CRFB1 from PKL cells (lane 1) and spleen cells (lane 2) and r*Lc*CRFB1-Ex (lane 3) and control (lane 4). The theoretical molecular masses of full-length *Lc*CRFB1 and *Lc*CRFB1-Ex are 59.62 and 22.76 kDa, respectively. **b**, Verification of anti–*Lc*CRFB1-Ex pAb specificity by immunofluorescence labeling in PKL and HEK-293T cells. The pCMV-HA plasmid was overexpressed in HEK-293T cells as control, and pCMV-HA-*Lc*CRFB1 containing full-length *Lc*CRFB1 cDNA was overexpressed in HEK-293T cells as the experimental group. (**B**) JAK1, IRF9, STAT1, and STAT2 and (**C**) MxA, PKR, and viperin expression levels upon receptor blockade with anti–*Lc*CRFB1-Ex, anti–*Lc*CRFB5-Ex, or both pAbs in *Lc*IFNd-stimulated PKLs. (**D**) STAT1 and STAT2 phosphorylation were inhibited by anti–*Lc*CRFB1-Ex, anti–*Lc*CRFB5-Ex, or both Abs in *Lc*IFNd-stimulated PKLs. Bars represent the means of three independent experiments ± SD. All experiments were performed in triplicate. Different lowercase letters indicate significant differences. $^{**}p < 0.01$.

The ancient and powerful host first-line antiviral defense strategy of the type I IFN system is conserved from mammals to teleosts (46). Zebrafish IFN-φ1–4 (20, 24), Atlantic salmon IFNa1 (47), grass carp IFNa (23, 48), and large yellow croaker IFNi (18, 25) have all been shown to induce antiviral response through the JAK-STAT signaling pathway. Our findings show that *Lc*IFNd also signals through this conserved pathway (Fig. 6). We further found that the *Lc*IFNd residues involved in receptor interaction (Supplemental Fig. 2C) are highly conserved in the members of fish type I subgroup d among other fish species, suggesting that the manner by which fish type I subgroup d IFNs bind to their receptors CRFB1 and CRFB5 is conserved. The mechanisms by which *Lc*IFNd binds to the receptors *Lc*CRFB1 and *Lc*CRFB5 and subsequently activates antiviral response through JAK-STAT signaling pathway are summarized in Fig. 8.

In summary, this study demonstrates that *Lc*CRFB1 and *Lc*CRFB5 are the functional receptors of *Lc*IFNd, reveals a ligand/receptor complex binding mechanism of IFNd in teleost fish, and suggests that the receptor binding mechanism is determined by structural differences between group I and group II IFNs of teleost type I IFNs. Our results thus provide new insights into function and evolution of type I IFNs.

Acknowledgments

We thank Prof. Qiwei Qin in South China Agricultural University for providing the GS cells and SGIV. We thank the beamline BL02-U1 of Shanghai Synchrotron Radiation Facility for the x-ray diffraction data collection. We thank our colleague V. Perčulija for scientific and language editing of the article.

phosphorylation levels in PKL cells at different time points during *Lc*IFNd stimulation. Right, Histograms represent relative protein expression and phosphorylation levels of STAT1 and STAT2. (**D**) GS cells were pretreated with r*Lc*IFNd at a final concentration of 50 ng/ml or PBS (control) for 2 h; then, the cells were infected with SGIV at a multiplicity of infection of 2. **a**, At 24 h postinfection, GS cells were observed for CPE using microscopy. **b**, At 12 and 24 h postinfection, the expression levels of MCP and VP19 genes were detected by real-time PCR and normalized to that of *Ec*β-actin. Bars represent the means of three independent experiments ± SD. All experiments were performed in triplicate. $^{*}p < 0.05$, $^{**}p < 0.01$ (unpaired Student *t* test).

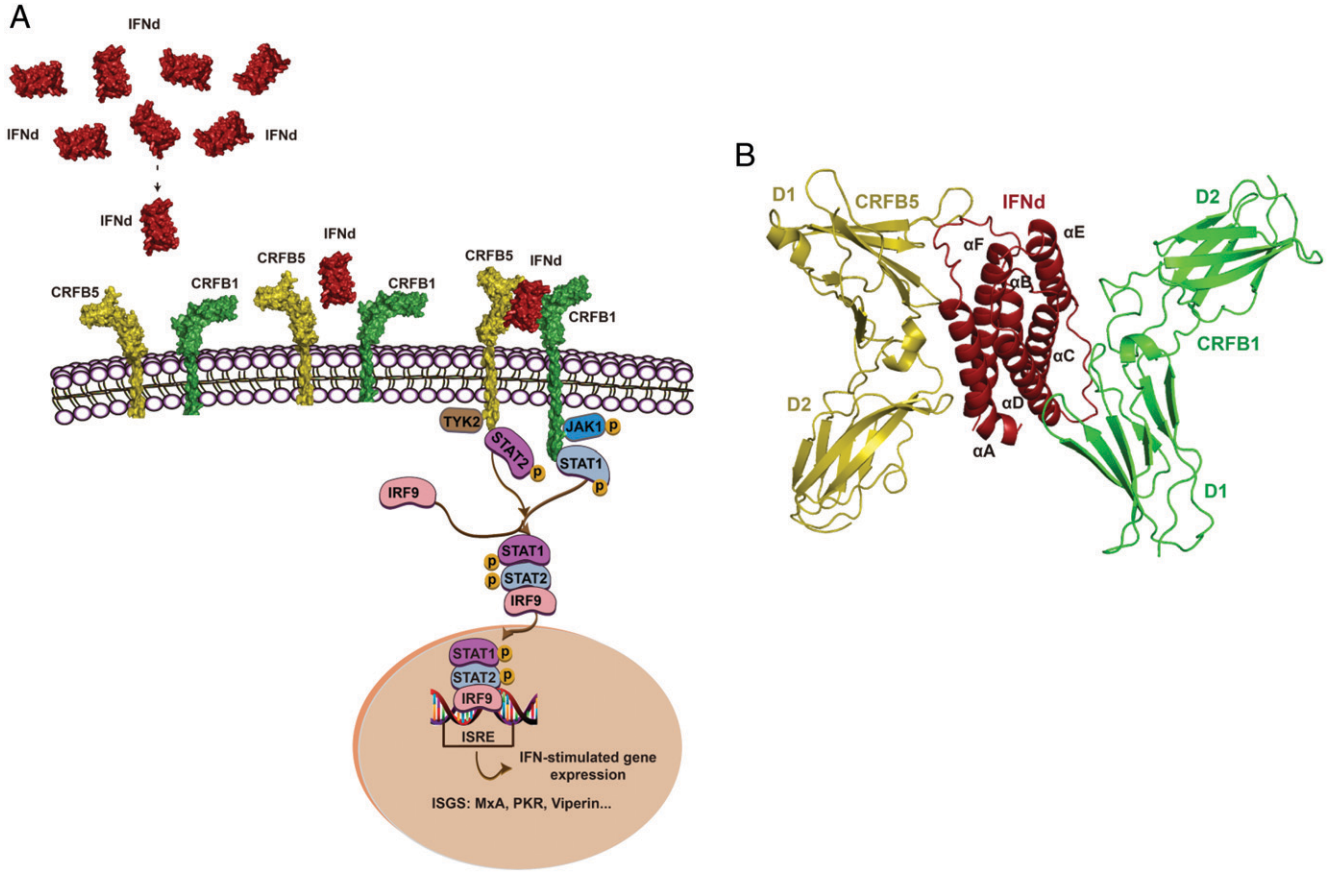

FIGURE 8. *Lc*IFNd signaling and ligand–receptor binding models. (**A**) The teleost fish type I group I IFNd binds to the surface receptor complex consisting of the receptor subunit CRFB5 and CRFB1, triggering the recruitment and activation of JAK1 and TYK2, which then phosphorylate STAT1 and STAT2, respectively. Phosphorylated STAT1 and STAT2 dimerize and assemble with IRF9 to form a transcription factor complex known as IFN-stimulated gene (ISG) factor 3 (ISGF3). ISGF3 then translocates to the nucleus and binds IFN-stimulated response elements (ISREs), activating the transcription of ISGs. (**B**) Cartoon representation of the structural model of the *Lc*IFNd–*Lc*CRFB1-Ex–*Lc*CRFB5-Ex complex.

Disclosures

The authors have no financial conflicts of interest.

References

1. Samuel, C. E. 2001. Antiviral actions of interferons. *Clin. Microbiol. Rev.* 14: 778–809.
2. Dunn, G. P., C. M. Koebel, and R. D. Schreiber. 2006. Interferons, immunity and cancer immunoediting. *Nat. Rev. Immunol.* 6: 836–848.
3. Borden, E. C., G. C. Sen, G. Uze, R. H. Silverman, R. M. Ransohoff, G. R. Foster, and G. R. Stark. 2007. Interferons at age 50: past, current and future impact on biomedicine. *Nat. Rev. Drug Discov.* 6: 975–990.
4. Pestka, S. 2007. The interferons: 50 years after their discovery, there is much more to learn. *J. Biol. Chem* 282: 20047–20051.
5. Piehler, J., and G. Schreiber. 1999. Biophysical analysis of the interaction of human ifnar2 expressed in *E. coli* with IFNα2. *J. Mol. Biol.* 289: 57–67.
6. Pestka, S., C. D. Krause, and M. R. Walter. 2004. Interferons, interferon-like cytokines, and their receptors. *Immunol. Rev.* 202: 8–32.
7. Jaks, E., M. Gavutis, G. Uzé, J. Martal, and J. Piehler. 2007. Differential receptor subunit affinities of type I interferons govern differential signal activation. *J. Mol. Biol.* 366: 525–539.
8. Briscoe, J., D. Guschin, N. C. Rogers, D. Watling, M. Müller, F. Horn, P. Heinrich, G. R. Stark, and I. M. Kerr. 1996. JAKs, STATs and signal transduction in response to the interferons and other cytokines. *Philos. Trans. R. Soc. B Biol. Soc.* 351: 167–171.
9. Platanias, L. C. 2005. Mechanisms of type-I- and type-II-interferon-mediated signalling. *Nat. Rev. Immunol.* 5: 375–386.
10. Chill, J. H., S. R. Quadt, R. Levy, G. Schreiber, and J. Anglister. 2003. The human type I interferon receptor: NMR structure reveals the molecular basis of ligand binding. *Structure* 11: 791–802.
11. Lamken, P., S. Lata, M. Gavutis, and J. Piehler. 2004. Ligand-induced assembling of the type I interferon receptor on supported lipid bilayers. *J. Mol. Biol.* 341: 303–318.
12. Roisman, L. C., D. A. Jaitin, D. P. Baker, and G. Schreiber. 2005. Mutational analysis of the IFNAR1 binding site on IFNα2 reveals the architecture of a weak ligand-receptor binding-site. *J. Mol. Biol.* 353: 271–281.
13. Li, Z., J. J. Strunk, P. Lamken, J. Piehler, and T. Walz. 2008. The EM structure of a type I interferon-receptor complex reveals a novel mechanism for cytokine signaling. *J. Mol. Biol.* 377: 715–724.
14. Thomas, C., I. Moraga, D. Levin, P. O. Krutzik, Y. Podoplelova, A. Trejo, C. Lee, G. Yarden, G. Yarden, J. S. Glenn, et al. 2011. Structural linkage between ligand discrimination and receptor activation by type I interferons. *Cell* 146: 621–632.
15. Robertsen, B., V. Bergan, T. Røkenes, R. Larsen, and A. Albuquerque. 2003. Atlantic salmon interferon genes: cloning, sequence analysis, expression, and biological activity. *J. Interferon Cytokine Res.* 23: 601–612.
16. Altmann, S. M., M. T. Mellon, D. L. Distel, and C. H. Kim. 2003. Molecular and functional analysis of an interferon gene from the zebrafish, *Danio rerio*. *J. Virol.* 77: 1992–2002.
17. Chang, M., P. Nie, B. Collet, C. J. Secombes, and J. Zou. 2009. Identification of an additional two-cysteine containing type I interferon in rainbow trout *Oncorhynchus mykiss* provides evidence of a major gene duplication event within this gene family in teleosts. *Immunogenetics* 61: 315–325.
18. Chen, J., Y. Guan, H. Guan, Y. Mu, Y. Ding, J. Zou, S. Ouyang, and X. Chen. 2022. Molecular and structural basis of receptor binding and signaling of a fish type I IFN with three disulfide bonds. *J. Immunol.* 209: 806–819.
19. Lutfalla, G., Roest, C. H. Stange-Tho, Mann, N. Jaillon, O. Mogensen, K, and Monneron, D. 2003. Comparative genomic analysis reveals independent expansion of a lineage-specific gene family in vertebrates: the class II cytokine receptors and their ligands in mammals and fish. *BMC Genomics* 4: 29.
20. Aggad, D., M. Mazel, P. Boudinot, K. E. Mogensen, O. J. Hamming, R. Hartmann, S. Kotenko, P. Herbomel, G. Lutfalla, and J. P. Levraud. 2009. The two groups of zebrafish virus-induced interferons signal via distinct receptors with specific and shared chains. *J. Immunol.* 183: 3924–3931.
21. Levraud, J. P., P. Boudinot, I. Colin, A. Benmansour, N. Peyrieras, P. Herbomel, and G. Lutfalla. 2007. Identification of the zebrafish IFN receptor: implications for the origin of the vertebrate IFN system. *J. Immunol.* 178: 4385–4394.
22. Laghari, Z. A., S. N. Chen, L. Li, B. Huang, Z. Gan, Y. Zhou, H. J. Huo, J. Hou, and P. Nie. 2018. Functional, signalling and transcriptional differences of three distinct type I IFNs in a perciform fish, the mandarin fish siniperca chuatsi. *Dev. Comp. Immunol.* 84: 94–108.
23. Wang, Z., J. Xu, J. Feng, K. Wu, K. Chen, Z. Jia, X. Zhu, W. Huang, X. Zhao, Q. Liu, et al. 2022. Structural and functional analyses of type I IFNa shed light into its interaction with multiple receptors in fish. *Front. Immunol.* 13: 862764.

24. Hamming, O. J., G. Lutfalla, J. P. Levraud, and R. Hartmann. 2011. Crystal structure of zebrafish interferons I and II reveals conservation of type I interferon structure in vertebrates. *J. Virol.* 85: 8181–8187.
25. Ding, Y., J. Ao, X. Huang, and X. Chen. 2016. Identification of two subgroups of type I IFNs in perciforme fish large yellow croaker *Larimichthys crocea* provides novel insights into function and regulation of fish type I IFNs. *Front. Immunol.* 7: 343.
26. Li, M., Q. Li, Z. Yang, G. Hu, T. Li, X. Chen, and J. Ao. 2014. Identification of cathepsin B from large yellow croaker (*Pseudosciaena crocea*) and its role in the processing of MHC class II-associated invariant chain. *Dev. Comp. Immunol.* 45: 313–320.
27. Wang, X., K. Wang, P. Nie, X. Chen, and J. Ao. 2014. Establishment and characterization of a head kidney cell line from large yellow croaker *Pseudosciaena crocea*. *J. Fish Biol.* 84: 1551–1561.
28. Wei, S., Y. Huang, X. Huang, and Q. Qin. 2015. Characterization of c-Jun from orange-spotted grouper, *Epinephelus coioides* involved in SGIV infection. *Fish Shellfish Immunol.* 43: 230–240.
29. Adams, P. D., P. V. Afonine, G. Bunkóczi, V. B. Chen, I. W. Davis, N. Echols, J. J. Headd, L. W. Hung, G. J. Kapral, R. W. Grosse-Kunstleve, et al. 2010. *PHENIX*: a comprehensive Python-based system for macromolecular structure solution. *Acta Crystallogr. D Biol. Crystallogr.* 66: 213–221.
30. Emsley, P., and K. Cowtan. 2004. *Coot*: model-building tools for molecular graphics. *Acta Crystallogr. D Biol. Crystallogr.* 60: 2126–2132.
31. Ao, J., Y. Mu, L. X. Xiang, D. Fan, M. Feng, S. Zhang, Q. Shi, L. Y. Zhu, T. Li, Y. Ding, et al. 2015. Genome sequencing of the perciform fish *Larimichthys crocea* provides insights into molecular and genetic mechanisms of stress adaptation. *PLoS. Genet.* 11: e1005118.
32. Neidhardt, F. C., P. L. Bloch, D. F. Smith, and D. F. 1974. Smith. Culture medium for enterobacteria. *J. Bacteriol.* 119: 736–747.
33. Zhang, Q., H. Zhang, F. Zheng, R. Liu, X. Liao, C. Guo, and D. Lin. 2021. ^{1}H, ^{13}C, ^{15}N backbone and side-chain resonance assignments of the pathogenic G131V mutant of human prion protein (91–231). *Biomol. NMR Assign.*15: 311–316.
34. Delaglio, F., S. Grzesiek, G. W. Vuister, G. Zhu, J. Pfeifer, and A. Bax. 1995. NMRPipe: a multidimensional spectral processing system based on UNIX pipes. *J. Biomol. NMR* 6: 277–293.
35. Lee, W., M. Tonelli, and J. L. Markley. 2015. NMRFAM-SPARKY: enhanced software for biomolecular NMR spectroscopy. *Bioinformatics* 31: 1325–1327.
36. Vilar, S., G. Cozza, and S. Moro. 2008. Medicinal chemistry and the Molecular Operating Environment (MOE): application of QSAR and molecular docking to drug discovery. *Curr. Top. Med. Chem.*8: 1555–1572.
37. Brymora, A., Valova, V. A., and Robinson, P. J. 2004. Protein-protein interactions identified by pull-down experiments and mass spectrometry. *Curr. Protoc. Cell. Biol.* Chapter 17: Unit 17.5.
38. Fu, Q., Z. Wei, Y. Chen, J. Xie, X. Zhang, T. He, and X. Chen. 2021. Development of monoclonal antibody against IgT of a perciform fish, large yellow croaker (*Larimichthys crocea*) and characterization of IgT^{+} B cells. *Dev. Comp. Immunol.* 119: 104027.
39. Mu, P., J. Huo, X. Li, W. Li, X. Li, J. Ao, and X. Chen. 2022. Il-2 signaling couples the MAPK and MTORC1 axes to promote T cell proliferation and differentiation in teleosts. *J. Immunol.* 208: 1616–1631.
40. Walter, M. R. 2004. Structural analysis of il-10 and type I interferon family members and their complexes with receptor. *Adv. Protein. Chem. Struct. Biol* 68: 171–223.
41. Wang, X., P. Lupardus, S. L. Laporte, and K. C. Garcia. 2009. Structural biology of shared cytokine receptors. *Annu. Rev. Immunol.* 27: 29–60.
42. Stein, C., M. Caccamo, G. Laird, and M. Leptin. 2007. Conservation and divergence of gene families encoding components of innate immune response systems in zebrafish. *Genome Biol.* 8: R251.
43. Stifter, S. A., A. Y. Matthews, N. E. Mangan, K. Y. Fung, A. Drew, M. D. Tate, T. P. Soares-da-Costa, D. Hampsey, J. Mayall, P. M. Hansbro, et al. 2018. Defining the distinct, intrinsic properties of the novel type I interferon, IFNϵ. *J. Biol. Chem.* 293: 3168–3179.
44. de Weerd, N. A., J. P. Vivian, T. K. Nguyen, N. E. Mangan, J. A. Gould, S.-J. Braniff, L. Zaker-Tabrizi, K. Y. Fung, S. C. Forster, T. Beddoe, et al. 2013. Structural basis of a unique interferon-β signaling axis mediated via the receptor IFNAR1. *Nat. Immunol.* 14: 901–907.
45. Senda, T., T. Shimazu, S. Matsuda, G. Kawano, H. Shimizu, K. T. Nakamura, and Y. Mitsui. 1992. Three-dimensional crystal structure of recombinant murine interferon-beta. *EMBO J.* 11: 3193–3201.
46. Sobhkhez, M., A. Skjesol, E. Thomassen, L. G. Tollersrud, L. G. Tollersrud, D. B. Iliev, B. Sun, B. Robertsen, and J. B. Jørgensen. 2014. Structural and functional characterization of salmon STAT1, STAT2 and IRF9 homologs sheds light on interferon signaling in teleosts. *FEBS. Open. Bio.*4: 858–871.
47. Skjesol, A., T. Liebe, D. B. Iliev, E. I. Thomassen, L. G. Tollersrud, M. Sobhkhez, L. Lindenskov- Joensen, C. J. Secombes, and J. B. Jørgensen. 2014. Functional conservation of suppressors of cytokine signaling proteins between teleosts and mammals: Atlantic salmon SOCS1 binds to JAK/STAT family members and suppresses type I and II IFN signaling. *Dev. Comp. Immunol.* 45: 177–189.
48. Hou, Q., R. Gong, X. Liu, H. Mao, X. Xu, D. Liu, Z. Dai, H. Wang, B. Wang, and C. Hu. 2017. Poly I:C facilitates the phosphorylation of *Ctenopharyngodon idellus* type I IFN receptor subunits and JAK kinase. *Fish Shellfish Immunol.* 60: 13–20.